Corso di Laurea in Ing. Elettrotecnica

Corso di Fisica II

Cenni di Fisica della superconduttività

Prof. A. Barra

A.A. 2012-13

Libro: Superconductivity and cryogenics for accelerators and detectors
School of Erice, Italy 2002

Capitolo 1: **Superconductivity**
1) Introduction

2) Meissner-Ochsenefeld effect and London equation

3) Thermodynamic properties of superconductors
-3.1: The superconducting phase (cenni)
-3.2: Energy balance in a magnetic field (cenni)
-3.3: Type II superconductors
-3.4: When a superconductor is type I or type II?
-3.5: Heat capacity and heat conductivity (cenni)

4) Basic concepts and results:
cenni

Per l'origine della resistenza ohmica (in approssimazione classica) consultare direttamente Mencuccini Silvestrini **Fisica II**.

CERN–2004–008
11 September 2004

Estratto dal volume

ORGANISATION EUROPÉENNE POUR LA RECHERCHE NUCLÉAIRE
CERN EUROPEAN ORGANIZATION FOR NUCLEAR RESEARCH

CAS CERN ACCELERATOR SCHOOL

SUPERCONDUCTIVITY AND CRYOGENICS FOR ACCELERATORS AND DETECTORS

Erice, Italy
8–17 May 2002

PROCEEDINGS

Editors: S. Russenschuck, G. Vandoni

GENEVA
2004

Superconductivity

Peter Schmüser
Institut für Experimentalphysik der Universität Hamburg

Abstract
Low-temperature superconductivity is treated at an introductory level. The topics include Meissner-Ochsenfeld effect and London equations, thermodynamic properties of the superconducting state, type I and II superconductors, flux quantisation, superconductors in microwave fields and superconducting quantum interference effects. Important experiments are discussed. The basic ideas of the BCS theory and its implications are outlined.

1. INTRODUCTION

In these lectures I want to give an introduction into the physical principles of superconductivity and its fascinating properties. More detailed accounts can be found in the excellent text books by W. Buckel [1] and by D.R. Tilley and J. Tilley [2]. Superconductivity was discovered [3] in 1911 by the Dutch physicist H. Kamerlingh Onnes, only three years after he had succeeded in liquefying helium. During his investigations on the conductivity of metals at low temperature he found that the resistance of a mercury sample dropped to an unmeasurably small value just at the boiling temperature of liquid helium. The original measurement is shown in Fig. 1. Kamerlingh Onnes called this totally unexpected phenomenon 'superconductivity' and this name has been retained since. The temperature at which the transition took place was called the *critical temperature* T_c. Superconductivity is observed in a large variety of materials but, remarkably, not in some of the best normal conductors like copper, silver and gold, except at very high pressures. This is illustrated in Fig. 2 where the resistivity of copper, tin and the 'high-temperature' superconductor $YBa_2Cu_3O_7$ is sketched as a function of temperature. Table 1 lists some important superconductors together with their critical temperatures at vanishing magnetic field.

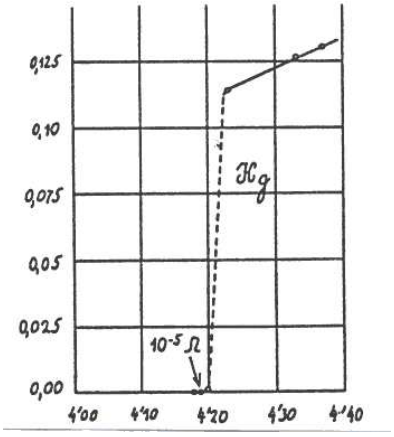

Fig. 1: The discovery of superconductivity by Kamerlingh Onnes.

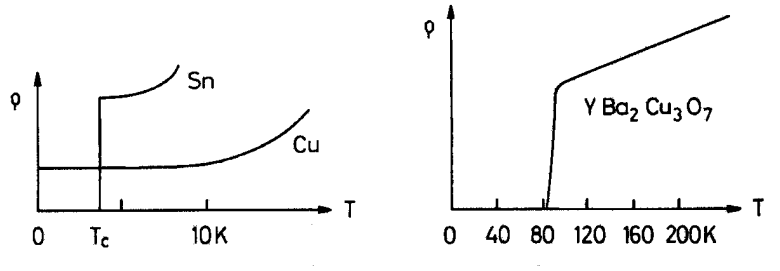

Fig. 2: The low-temperature resistivity of copper, tin and $YBa_2Cu_3O_7$.

Table 1: The critical temperature of some common materials at vanishing magnetic fi eld.

material	Ti	Al	Hg	Sn	Pb	Nb	NbTi	Nb_3Sn
T_c [K]	0.4	1.14	4.15	3.72	7.9	9.2	9.2	18

A conventional resistance measurement is far too insensitive to establish infinite conductivity, a much better method consists in inducing a current in a ring and determining the decay rate of the produced magnetic field. A schematic experimental setup is shown in Fig. 3. A bar magnet is inserted in the still normal-conducting ring and removed after cooldown below T_c. The induced current should decay exponentially

$$I(t) = I(0)\exp(-t/\tau)$$

with the time constant given by the ratio of inductivity and resistance, $\tau = L/R$, which for a normal metal ring is in the order of 100 μs. In superconducting rings, however, time constants of up to 10^5 years have been observed [4] so the resistance must be at least 15 orders of magnitude below that of copper and is indeed indistinguishable from zero. An important practical application of this method is the operation of solenoid coils for magnetic resonance imaging in the short-circuit mode which exhibit an extremely slow decay of the field of typically $3 \cdot 10^{-9}$ per hour [5].

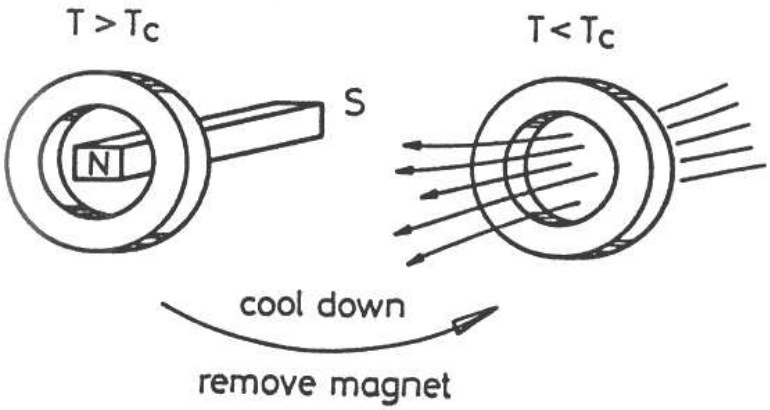

Fig. 3: Induction of a persistent current in a superconducting ring.

There is an intimate relation between superconductivity and magnetic fields. W. Meissner and R. Ochsenfeld [6] discovered in 1933 that a superconducting element like lead completely expelled a weak magnetic field from its interior when cooled below T_c while in strong fields superconductivity broke down and the material went to the normal state. The spontaneous exclusion of magnetic fields upon crossing T_c could not be explained in terms of the Maxwell equations and indeed turned out to be a non-classical phenomenon. Two years later, H. and F. London [7] proposed an equation which offered a phenomenological explanation of the Meissner-Ochsenfeld effect but the justification of the London equation remained obscure until the advent of the Bardeen, Cooper and Schrieffer theory [8] of superconductivity in 1957. The BCS theory revolutionized our understanding of this fascinating phenomenon. It is based on the assumption that the supercurrent is not carried by single electrons but rather by pairs of electrons of opposite momenta and spins, the so-called *Cooper pairs*. All pairs occupy a single quantum state, the BCS ground state, whose energy is separated from the single-electron states by an energy gap which in turn can be related to the critical temperature. The BCS theory has turned out to be of enormous predictive power and many of its predictions and implications like the temperature dependence of the energy gap and its relation to the critical temperature, the quantisation of magnetic flux and the existence of quantum interference phenomena have been confirmed by experiment and, in many cases, even found practical application.

A discovery of enormous practical consequences was the finding that there exist two types of superconductors with rather different response to magnetic fields. The elements lead, mercury, tin, aluminium and others are called 'type I' superconductors. They do not admit a magnetic field in the bulk material and are in the superconducting state provided the applied field is below a *critical field* H_c which is a function of temperature. All superconducting alloys like lead-indium, niobium-titanium, niobium-tin and also the element niobium belong to the large class of 'type II' superconductors. They are characterized by two critical fields, H_{c1} and H_{c2}. Below H_{c1} these substances are in the *Meissner phase* with complete field expulsion while in the range $H_{c1} < H < H_{c2}$ a type II superconductor enters the *mixed phase* in which magnetic field can penetrate the bulk material in the form of flux tubes. The Ginzburg-Landau theory [9] provides a theoretical basis for the distinction between the two types. Around 1960 Gorkov [10] showed that the phenomenological Ginzburg-Landau theory is a limiting case of the BCS theory. Abrikosov [11] predicted that the flux tubes in a type II superconductor arrange themselves in a triangular pattern which was confirmed in a beautiful experiment by Essmann and Träuble [12]. In 1962 Josephson [13] studied the quantum theoretical tunnel effect in a system of two superconductors separated by a thin insulating layer and he predicted peculiar and fascinating properties of such a *Josephson junction* which were all confirmed by experiment and opened the way to superconducting quantum interference devices (SQUID's) with extreme sensitivity to tiny magnetic fields.

2. MEISSNER-OCHSENFELD EFFECT AND LONDON EQUATION

We consider a cylinder with perfect conductivity and raise a magnetic field from zero to a finite value H. A surface current is induced whose magnetic field, according to Lenz's rule, is opposed to the applied field and cancels it in the interior. Since the resistance is zero the current will continue to flow with constant strength as long as the external field is kept constant and consequently the bulk of the cylinder will stay field-free. This is exactly what happens if we expose a lead cylinder in the superconducting state ($T < T_c$) to an increasing field, see the path $(a) \rightarrow (c)$ in Fig. 4. So below T_c lead acts as a perfect diamagnetic material. There is, however, another path leading to the point (c). We start with a lead cylinder in the normal state ($T > T_c$) and expose it to a field which is increased from zero to H. Eddy currents are induced in this case as well but they decay rapidly and after a few hundred microseconds the field lines will fully penetrate the material (state (b) in Fig. 4). Now the cylinder is cooled down. At the very instant the temperature drops below T_c , a surface current is spontaneously created and the magnetic field is expelled from the interior of the cylinder. This surprising observation is called the

Meissner-Ochsenfeld effect after its discoverers; it cannot be explained by the law of induction because the magnetic field is kept constant.

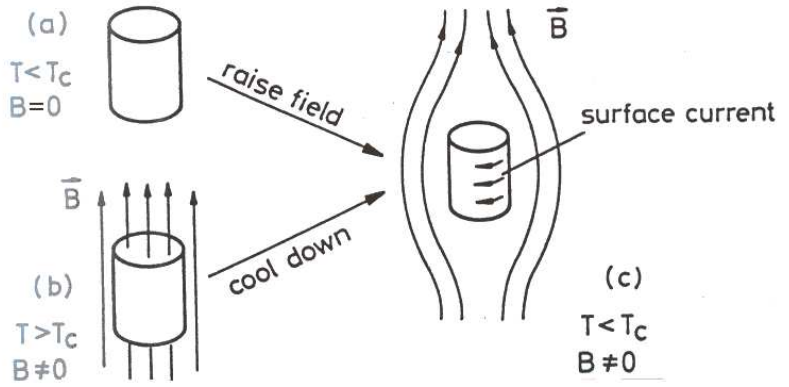

Fig. 4: A lead cylinder in a magnetic fi eld. Two possible ways to reach the superconducting fi nal state with $H > 0$ are sketched. Ideally the length of the cylinder should be much larger than its diameter to get a vanishing demagnetisation factor.

In a (T, H) plane, the superconducting phase is separated from the normal phase by the curve $H_c(T)$ as sketched in Fig. 5. Also indicated are the two ways on which one can reach the point (c). It is instructive to compare this with the response of a 'normal' metal of perfect conductivity. The field increase along the path $(a) \rightarrow (c)$ would yield the same result as for the superconductor, however the cooldown along the path $(b) \rightarrow (c)$ would have no effect at all. So superconductivity means definitely more than just vanishing resistance.

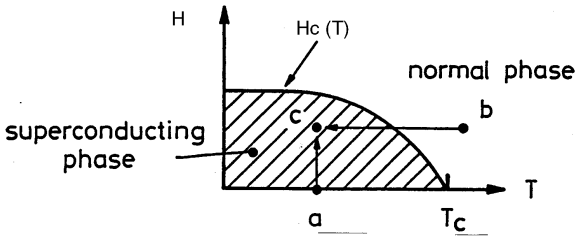

Fig. 5: The phase diagram in a (T, H) plane.

I have already used the terms 'superconducting phase' and 'normal phase' to characterize the two states of lead. These are indeed phases in the thermodynamical sense, comparable to the different phases of H_2O which is in the solid, liquid or gaseous state depending on the values of the parameters temperature and pressure. Here the relevant parameters are temperature and magnetic field (for some materials also pressure). If the point (T, H) lies below the curve $H_c(T)$ the material is superconducting and expels the magnetic field, irrespective of by which path the point was reached. If (T, H) is above the curve the material is normal-conducting.

The first successful explanation of the Meissner-Ochsenfeld effect was achieved in 1935 by Heinz and Fritz London. They assumed that the supercurrent is carried by a fraction of the conduction electrons in the metal. The 'super-electrons' experience no friction, so their equation of motion in an electric field is

$$m_e \frac{\partial \vec{v}}{\partial t} = -e\vec{E} \; .$$

This leads to an accelerated motion. The supercurrent density is

$$\vec{J}_s = -en_s\vec{v}$$

where n_s is the density of the super-electrons. This immediately yields the equation

$$\frac{\partial \vec{J}_s}{\partial t} = \frac{n_s e^2}{m_e}\vec{E}\ . \tag{1}$$

Now one uses the Maxwell equation

$$\vec{\nabla} \times \vec{E} = -\frac{\partial \vec{B}}{\partial t}$$

and takes the curl (rotation) of (1) to obtain

$$\frac{\partial}{\partial t}\left(\frac{m_e}{n_s e^2}\vec{\nabla} \times \vec{J}_s + \vec{B}\right) = 0\ .$$

Since the time derivative vanishes the quantity in the brackets must be a constant. Up to this point the derivation is fully compatible with classical electromagnetism, applied to the frictionless acceleration of electrons. An example might be the motion of electrons in the vacuum of a television tube or in a circular accelerator. The essential new assumption H. and F. London made is that the bracket is not an arbitrary constant but is identical to zero. Then one obtains the important London equation

$$\vec{\nabla} \times \vec{J}_s = -\frac{n_s e^2}{m_e}\vec{B}\ . \tag{2}$$

It should be noted that this assumption cannot be justified within classical physics, even worse, in general it is wrong. For instance the current density in a normal metal will vanish when no electric field is applied, and whether a static magnetic field penetrates the metal is of no importance. In a superconductor of type I, on the other hand, the situation is such that Eq. (2) applies. Combining the fourth Maxwell equation (for time-independent fields)

$$\vec{\nabla} \times \vec{B} = \mu_0 \vec{J}_s$$

and the London equation and making use of the relation

$$\vec{\nabla} \times (\vec{\nabla} \times \vec{B}) = -\nabla^2 \vec{B}$$

(this is valid since $\vec{\nabla} \cdot \vec{B} = 0$) we get the following equation for the magnetic field in a superconductor

$$\nabla^2 \vec{B} - \frac{\mu_0 n_s e^2}{m_e}\vec{B} = 0\ . \tag{3}$$

It is important to note that this equation is not valid in a normal conductor. In order to grasp the significance of Eq. (3) we consider a simple geometry, namely the boundary between a superconducting half space and vacuum, see Fig. 6a. Then, for a magnetic field parallel to the surface, Eq. (3) becomes

$$\frac{d^2 B_y}{dx^2} - \frac{1}{\lambda_L^2}B_y = 0$$

with the solution

$$B_y(x) = B_0 \exp(-x/\lambda_L)\ .$$

Here we have introduced a very important superconductor parameter, the *London penetration depth*

$$\lambda_L = \sqrt{\frac{m_e}{\mu_0 n_s e^2}}\quad . \tag{4}$$

So the magnetic field does not stop abruptly at the superconductor surface but penetrates into the material with exponential attenuation. For typical material parameters the penetration depth is quite small, 20 – 50 nm. In the bulk of a thick superconductor there can be no magnetic field, which is just the Meissner-Ochsenfeld effect. Here it is appropriate to remark that in the BCS theory not single electrons but pairs of electrons are the carriers of the supercurrent. Their mass is $m_c = 2m_e$, their charge $-2e$, their density $n_c = n_s/2$. Obviously the penetration depth remains unchanged when going from single electrons to Cooper pairs.

We have now convinced ourselves that the superconductor can tolerate a magnetic field only in a thin surface layer (this is the case for type I superconductors). An immediate consequence is that current flow is restricted to the same thin layer. Currents in the interior are forbidden as they would generate magnetic fields in the bulk. The magnetic field and the current which are caused by an external field parallel to the axis of a lead cylinder are plotted in Fig. 6b. Another interesting situation occurs if we pass a current through a lead wire (Fig. 6c). It flows only in a very thin surface sheet of about 20 nm thickness, so the overall current in the wire is small. This is a first indication that type I superconductors are not suitable for winding superconducting magnet coils.

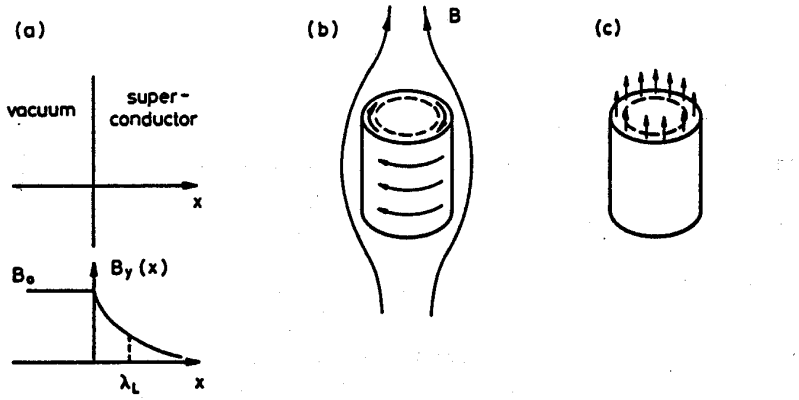

Fig. 6: (a) Exponential attenuation of a magnetic fi eld in a superconducting half plane. (b) Shielding current in a superconducting cylinder induced by a fi eld parallel to the axis. (c) A current-carrying wire made from a type I superconductor.

The penetration depth has a temperature dependence which can be calculated in the BCS theory. When approaching the critical temperature, the density of the supercurrent carriers goes to zero, so λ_L must become infinite:

$$\lambda_L \to \infty \quad \text{for} \quad T \to T_c \; .$$

This is shown in Fig. 7. An infinite penetration depth means no attenuation of a magnetic field which is just what one observes in a normal conductor.

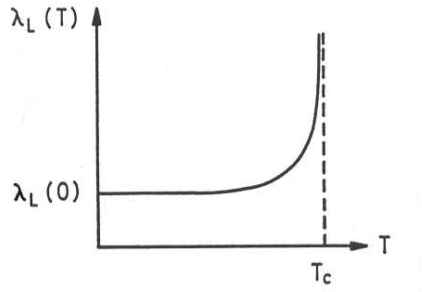

Fig. 7: Temperature dependence of the London penetration depth.

3. THERMODYNAMIC PROPERTIES OF SUPERCONDUCTORS

3.1 The superconducting phase

A material like lead goes from the normal into the superconducting state when it is cooled below T_c and when the magnetic field is less than $H_c(T)$. It has been mentioned already that this is a phase transition comparable to the transition from water to ice at $0°$C and normal pressure. Phase transitions take place when the new state is energetically favoured. The relevant thermodynamic energy is here the Gibbs free energy (see Appendix A)

$$G = U - T\,S - \mu_0 \vec{M} \cdot \vec{H} \tag{5}$$

where U is the internal energy, S the entropy and M the magnetisation of the superconductor (the magnetic moment per unit volume). A measurent of the free energy of aluminium is shown in Fig. 8a. Below T_c the superconducting state has a lower free energy than the normal state and thus the transition normal $\rightarrow$ superconducting is associated with a gain in energy. The entropy of the superconducting state is lower because there is a higher degree of order in this state. From the point of view of the BCS theory this is quite understandable since the conduction electrons are paired and collect themselves in a single quantum state. Numerically the entropy difference is small, though, about 1 milli-Joule per mole and Kelvin, from which one can deduce that only a small fraction of the valence electrons of aluminium is condensed into Cooper pairs. It should be noted, that also normal conduction is carried by just a small fraction of the valence electrons, see sect. 4.1.

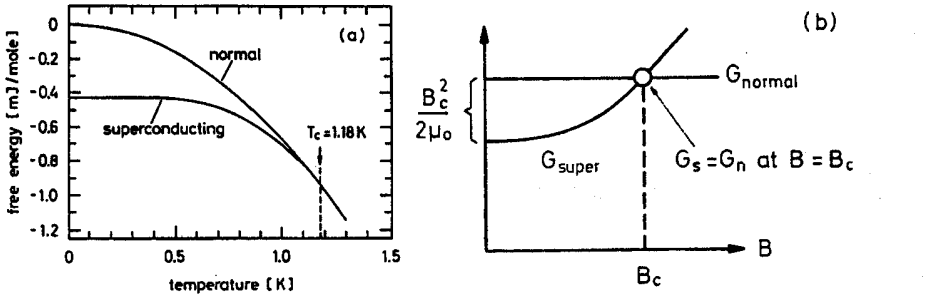

Fig. 8: (a) Free energy of aluminium in the normal and superconducting state as a function of T (after N.E. Phillips). The normal state was achieved by exposing the sample to a field larger than H_c while the superconducting state was measured at $H = 0$. (b) Schematic sketch of the free energies G_{norm} and G_{sup} as a function of the applied field $B = \mu_0 H$.

3.2 Energy balance in a magnetic field

We have argued that a lead cylinder becomes superconductive for $T < T_c$ because the free energy is reduced that way:

$$G_{sup} < G_{norm} \text{ for } T < T_c \ .$$

What happens if we apply a magnetic field? A normal-conducting metal cylinder is penetrated by the field so its free energy does not change: $G_{norm}(H) = G_{norm}(0)$. In contrast to this, a superconducting cylinder is strongly affected by the field. It sets up shielding currents which generate a magnetic moment $\vec{m}$ antiparallel to the applied field. The magnetic moment has a positive potential energy in the magnetic field

$$E_{pot} = -\mu_0 \, \vec{m} \cdot \vec{H} = +\mu_0 \, |\vec{m}| \, |\vec{H}| \ . \tag{6}$$

In the following it is useful to introduce the magnetisation M as the magnetic moment per unit volume. The magnetisation of a superconductor inside a current-carrying coil resembles that of an iron core. The 'magnetising' field H is generated by the coil current only and is unaffected by the presence of a magnetic material while the magnetic flux density[1] B is given by the superposition of H and the superconductor magnetisation M:

$$\vec{B} = \mu_0(\vec{H} + \vec{M}) \ . \tag{7}$$

In the following I will call both H and B magnetic fields. For a type I superconductor we have

$$\vec{M}(\vec{H}) = -\vec{H} \quad \text{and } \vec{B} = 0 \tag{8}$$

as long as $H < H_c$. The potential energy per unit volume is obtained by integration

$$E_{pot} = -\mu_0 \int_0^H \vec{M}(\vec{H}') \cdot d\vec{H}' = \mu_0 \int_0^H H'^2 dH' = \frac{\mu_0}{2} H^2 \ . \tag{9}$$

This corresponds to the increase in the Gibbs free energy that is caused by the magnetic field, see Fig. 8b.

$$G_{sup}(H) = G_{sup}(0) + \frac{\mu_0}{2} H^2 \ . \tag{10}$$

Here and in the following G denotes the Gibbs free energy per unit volume. The *critical field* is achieved when the free energy in the superconducting state just equals the free energy in the normal state

$$\frac{\mu_0}{2} H_c^2 = G_{norm} - G_{sup}(0) \ . \tag{11}$$

Since the energy density stored in a magnetic field is $(\mu_0/2)H^2$, an alternative interpretation of Eq. (11) is the following: in order to go from the normal to the superconducting state the material has to push out the magnetic energy, and the largest amount it can push out is the difference between the two free energies at vanishing field. For $H > H_c$ the normal phase has a lower energy, so superconductivity breaks down.

[1] There is often a confusion whether the H or the B field should be used. Unfortunately, much of the superconductivity literature is based on the obsolete CGS system of units where the distinction between B and H is not very clear and the two fields have the same dimension although their units were given different names: Gauss and Oerstedt.

3.3 Type II superconductors

For practical application in magnets it would be rather unfortunate if only type I superconductors existed which permit no magnetic field and no current in the bulk material. Alloys and the element niobium are so-called type II superconductors. Their magnetisation curves exhibit a more complicated dependence on magnetic field (Fig. 9). Type II conductors are characterized by two critical fields, H_{c1} and H_{c2}, which are both temperature dependent. For fields $0 < H < H_{c1}$ the substance is in the *Meissner phase* with complete exclusion of the field from the interior. In the range $H_{c1} < H < H_{c2}$ the substance enters the *mixed phase*, often also called Shubnikov phase: part of the magnetic flux penetrates the bulk of the sample. Above H_{c2}, finally, the material is normal-conducting. The area under the curve $M = M(H)$ is the same as for a type I conductor as it corresponds to the free-energy difference between the normal and the superconducting state and is given by $(\mu_0/2)\, H_c^2$.

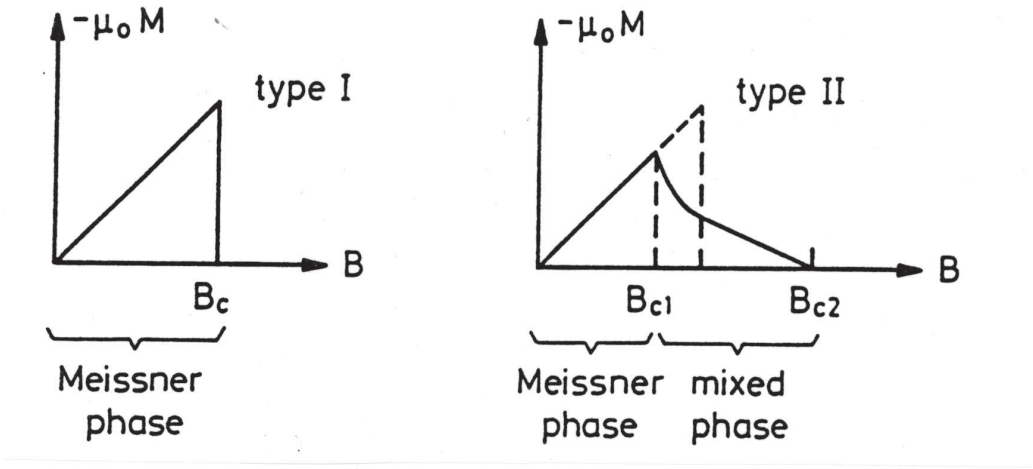

Fig. 9: Magnetisation of type I and type II superconductors as a function of the magnetic field.

It is instructive to compare measured data on pure lead (type I) and lead-indium alloys (type II) of various composition. Figure 10 shows that the upper critical field rises with increasing indium content; for Pb-In(20.4%) it is about eight times larger than the critical field of pure lead. Under the assumption that the free-energy difference is the same for the various lead-indium alloys, the areas under the three curves A, B, C in Fig. 10 should be identical as the diagram clearly confirms.

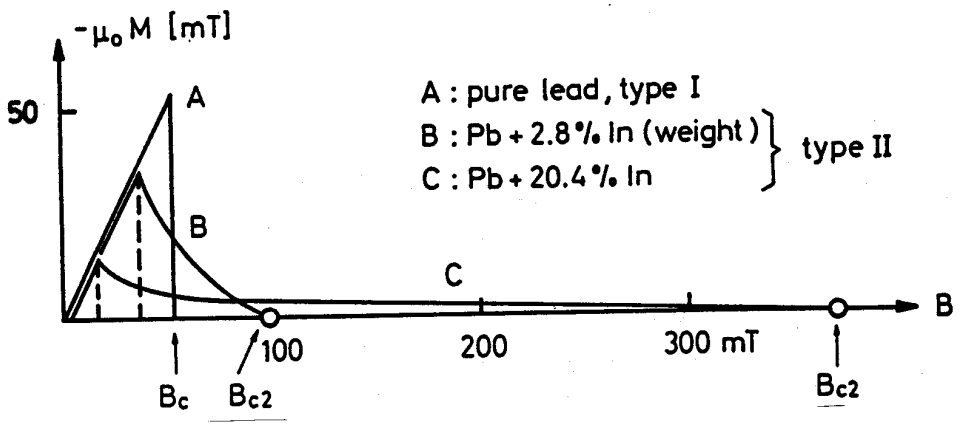

Fig. 10: The measured magnetisation curves [14] of lead-indium alloys of various composition, plotted against $B = \mu_0 H$.

A remarkable feature, which will be addressed in more detail later, is the observation that the magnetic flux does not penetrate the type II conductor with uniform density. Rather it is concentrated in *flux tubes* as sketched in Fig. 11. Each tube is surrounded with a super-vortex current. The material in between the tubes is field- and current-free.

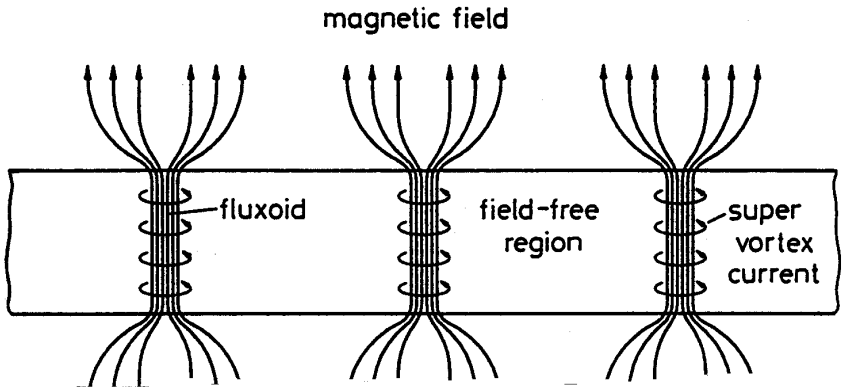

Fig. 11: Flux tubes in a type II superconductor.

The fact that alloys stay superconductive up to much higher fields is easy to understand: magnetic flux is allowed to penetrate the sample and therefore less magnetic field energy has to be driven out. Figure 12 shows that a type II superconducting cylinder in the mixed phase has a smaller magnetic moment than a type I cylinder. This implies that the curve $G_{sup}(H)$ reaches the level $G_{sup}(H) = G_{norm}$ at a field $H_{c2} > H_c$.

In a (T, H) plane the three phases of a type II superconductor are separated by the curves $H_{c1}(T)$ and $H_{c2}(T)$ which meet at $T = T_c$, see Fig. 13a. The upper critical field can assume very large values which make these substances extremely interesting for magnet coils (Fig. 13b).

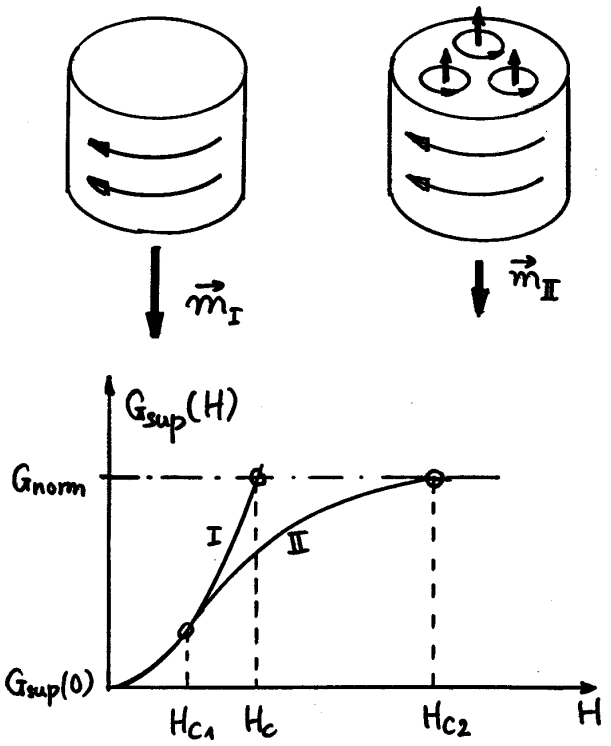

Fig. 12: Top: Magnetic moment of a type I and a type II sc cylinder in a field $H_{c1} < H < H_c$. Bottom: The Gibbs free energies of both cylinders as a function of field.

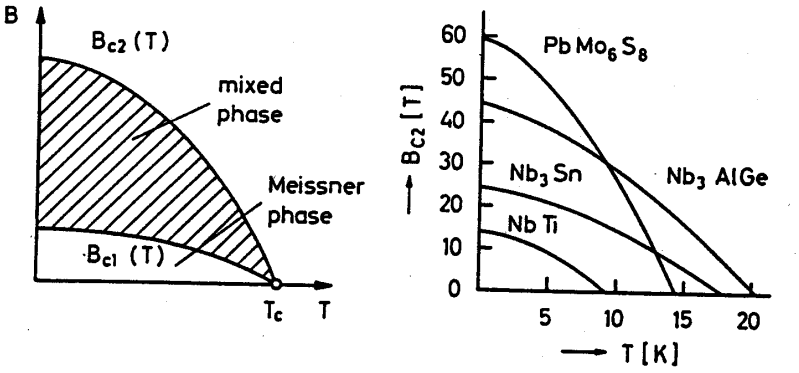

Fig. 13: (a) The phase diagram of a type II superconductor. (b) The upper critical field $B_{c2} = \mu_0 H_{c2}$ of several high-field alloys as a function of temperature.

3.4 When is a superconductor of type I or type II?

3.41 Thin sheets of type I superconductors

Let us first stick to type I conductors and compare the magnetic properties of a very thin sheet (thickness $d < \lambda_L$) to those of a thick slab. The thick slab has a vanishing B field in the bulk (Fig. 14a) while in the

thin sheet (Fig. 14b) the B field does not drop to zero at the centre. Consequently less energy needs to be expelled which implies that the critical field of a very thin sheet is much larger than the B_c of a thick slab. From this point of view it might appear energetically favourable for a thick slab to subdivide itself into an alternating sequence of thin normal and superconducting slices as indicated in Fig. 14c. The magnetic energy is indeed lowered that way but there is another energy to be taken into consideration, namely the energy required to create the normal-superconductor interfaces. A subdivision is only sensible if the interface energy is less than the magnetic energy.

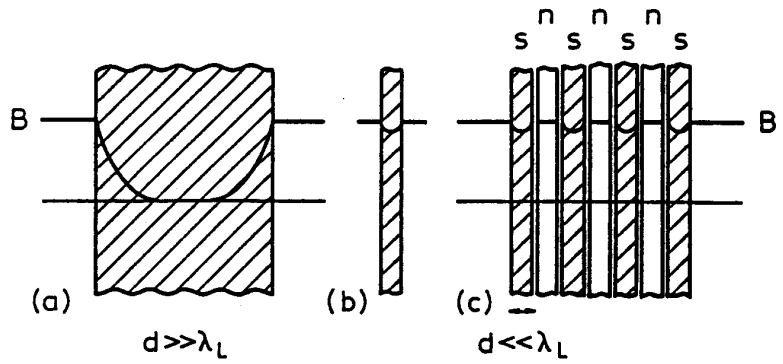

Fig. 14: Attenuation of field (a) in a thick slab and (b) in thin sheet. (c) Subdivision of a thick slab into alternating layers of normal and superconducting slices.

3.42 Coherence length

At a normal-superconductor boundary the density of the supercurrent carriers (the Cooper pairs) does not jump abruptly from zero to its value in the bulk but rises smoothly over a finite length ξ, the coherence length, see Fig. 15.

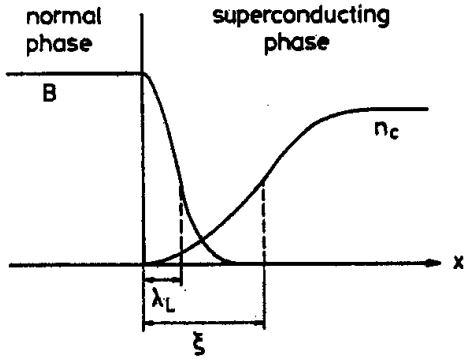

Fig. 15: The exponential drop of the magnetic field and the rise of the Cooper-pair density at a boundary between a normal and a superconductor.

The relative size of the London penetration depth and the coherence length decides whether a material is a type I or a type II superconductor. To study this in a semi-quantitative way, we first define the *thermodynamic critical field* by the energy relation

$$\frac{\mu_0}{2}H_c^2 = G_{norm} - G_{sup}(0)\ . \tag{12}$$

For type I this coincides with the known H_c, see Eq. (11), while for type II conductors H_c lies between H_{c1} and H_{c2}. The difference between the two free energies, $G_{norm} - G_{sup}(0)$, can be intepreted as the Cooper-pair condensation energy.

For a conductor of unit area, exposed to a field $H = H_c$ parallel to the surface, the energy balance is as follows:
(a) The magnetic field penetrates a depth λ_L of the sample which corresponds to an energy gain since magnetic energy must not be driven out of this layer:

$$\Delta E_{magn} = \frac{\mu_0}{2} H_c^2 \, \lambda_L \ . \tag{13}$$

(b) On the other hand, the fact that the Cooper-pair density does not assume its full value right at the surface but rises smoothly over a length ξ implies a loss of condensation energy

$$\Delta E_{cond} = -\frac{\mu_0}{2} H_c^2 \, \xi \ . \tag{14}$$

Obviously there is a net gain if $\lambda_L > \xi$. So a subdivision of the superconductor into an alternating sequence of thin normal and superconducting slices is energetically favourable if the London penetration depth exceeds the coherence length.

A more refined treatment is provided by the Ginzburg-Landau theory [9]. Here one introduces the *Ginzburg-Landau parameter*

$$\kappa = \lambda_L / \xi \ . \tag{15}$$

The criterion for type I or II superconductivity is found to be

$$\begin{array}{rl} \text{type I:} & \kappa < 1/\sqrt{2} \\ \text{type II:} & \kappa > 1/\sqrt{2}. \end{array}$$

In reality a type II superconductor is not subdivided into thin slices but the field penetrates the sample in flux tubes which arrange themselves in a triangular pattern. The core of a flux tube is normal. The following table lists the penetration depths and coherence lengths of some important superconducting elements. Niobium is a type II conductor but close to the border to type I, while indium, lead and tin are clearly type I conductors.

material	In	Pb	Sn	Nb
λ_L [nm]	24	32	≈ 30	32
ξ [nm]	360	510	≈ 170	39

The coherence length ξ is proportional to the mean free path ℓ of the conduction electrons in the metal. This quantity can be large for a very pure crystal but is strongly reduced by lattice defects and impurity atoms. In alloys the mean free path is generally much shorter than in pure metals so alloys are always type II conductors. In the Ginzburg-Landau theory the upper critical field is given by

$$B_{c2} = \sqrt{2}\, \kappa \, B_c = \frac{\Phi_0}{2\pi \xi^2} \tag{16}$$

where Φ_0 is the flux quantum (see sect. 5.2). For niobium-titanium with an upper critical field $B_{c2} = 10$ T at 4.2 K this formula yields $\xi = 6$ nm. The coherence length is larger than the typical width of a grain boundary in NbTi which means that the supercurrent can move freely from grain to grain. In high-T_c superconductors the coherence length is often shorter than the grain boundary width, and then current flow from one grain to the next is strongly impeded. There exists no simple expression for the lower critical field. In the limit $\kappa \gg 1$ one gets

$$B_{c1} = \frac{1}{2\kappa} (\ln \kappa + 0.08) B_c \ . \tag{17}$$

3.5 Heat capacity and heat conductivity

The specific heat capacity per unit volume at low temperatures is given by the expression

$$C_V(T) = \gamma T + A T^3 \; . \tag{18}$$

The linear term in T comes from the conduction electrons, the cubic term from lattice vibrations. The coefficients can be calculated within the free-electron-gas model and the Debye theory of lattice specific heat (see any standard textbook on solid state physics):

$$\gamma = \frac{\pi^2 n k_B^2}{2E_F} \; , \quad A = \frac{12\pi^4 N k_B}{5\Theta_D^3} \; . \tag{19}$$

Here $k_B = 1.38 \cdot 10^{-23}$ J/K is the Boltzmann constant, E_F the Fermi energy, n the density of the free electrons, N the density of the lattice atoms and Θ_D the Debye temperature of the material. If one plots the ratio $C(T)/T$ as a function of T^2 a straight line is obtained as can be seen in Fig. 16a for normal-conducting gallium [15]. In the superconducting state the electronic specific heat is different because the electrons bound in Cooper pairs no longer contribute to energy transport. In the BCS theory one expects an exponential rise of the electronic heat capacity with temperature

$$C_{e,s}(T) = 8.5\,\gamma\,T_c\,\exp(-1.44\,T_c/T) \tag{20}$$

The experimental data (Fig. 16a, b) are in good agreement with this prediction. There is a resemblance to the exponential temperature dependence of the electrical conductivity in intrinsic semiconductors and these data can be taken as an indication that an energy gap exists also in superconductors.

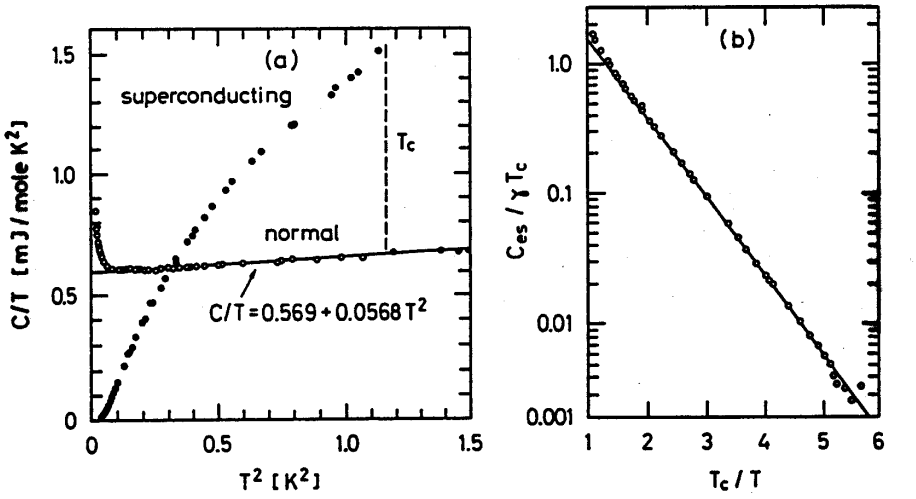

Fig. 16: (a) Specifi c heat $C(T)/T$ of normal and superconducting gallium as a function of T^2 [15]. (b) Experimental verifi cation of Eq. (20).

The heat conductivity of niobium is of particular interest for superconducting radio frequency cavities. Here the theoretical predictions are rather imprecise and measurements are indispensible. The low temperature values depend strongly on the *residual resistivity ratio* $RRR = R(300\,\mathrm{K})/R(10\,\mathrm{K})$ of the normal-conducting niobium. Figure 17 shows experimental data [16].

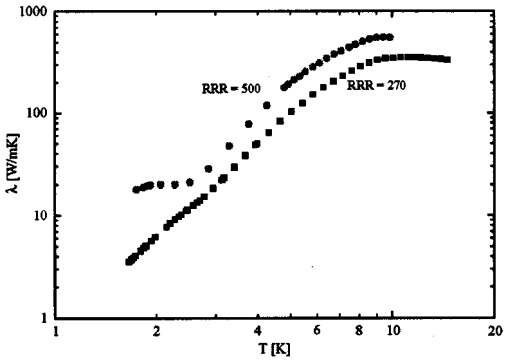

Fig. 17: Measured heat conductivity in niobium samples with $RRR = 270$ and $RRR = 500$ as a function of temperature [16].

4. BASIC CONCEPTS AND RESULTS OF THE BCS THEORY

4.1 The 'free electron gas' in a normal metal

4.11 The Fermi sphere

In a metal like copper the positively charged ions form a regular crystal lattice. The valence electrons (one per Cu atom) are not bound to specific ions but can move through the crystal. In the simplest quantum theoretical model the Coulomb attraction of the positive ions is represented by a potential well with a flat bottom, the periodic structure is neglected (taking into account the periodic lattice potential leads to the electronic band structure of semiconductors). The energy levels are computed by solving the Schrödinger equation with boundary conditions, and then the electrons are placed on these levels paying attention to the Pauli exclusion principle: no more than two electrons of opposite spin are allowed on each level. The electrons are treated as independent and non-interacting particles, their mutual Coulomb repulsion is taken into account only globally by a suitable choice of the depth of the potential well. It is remarkable that such a simple-minded picture of a 'free electron gas' in a metal can indeed reproduce the main features of electrical and thermal conduction in metals. However, an essential prerequisite is to apply the Fermi-Dirac statistics, based on the Pauli principle, and to avoid the classical Boltzmann statistics which one uses for normal gases. The electron gas has indeed rather peculiar properties. The average kinetic energy of the metal electrons is by no means given by the classical expression

$$\frac{m_e}{2}\,\overline{v^2} = \frac{3}{2}k_B T$$

which amounts to about 0.025 eV at room temperature. Instead, the energy levels are filled with two electrons each up to the Fermi energy E_F. Since the electron density n is very high in metals, E_F assumes large values, typically 5 eV. The average kinetic energy of an electron is $3/5E_F \approx 3$ eV and thus much larger than the average energy of a usual gas molecule. The electrons constitute a system called a 'highly degenerate' Fermi gas. The Fermi energy is given by the formula

$$E_F = \frac{\hbar^2}{2m_e}(3\pi^2 n)^{2/3}\ . \tag{21}$$

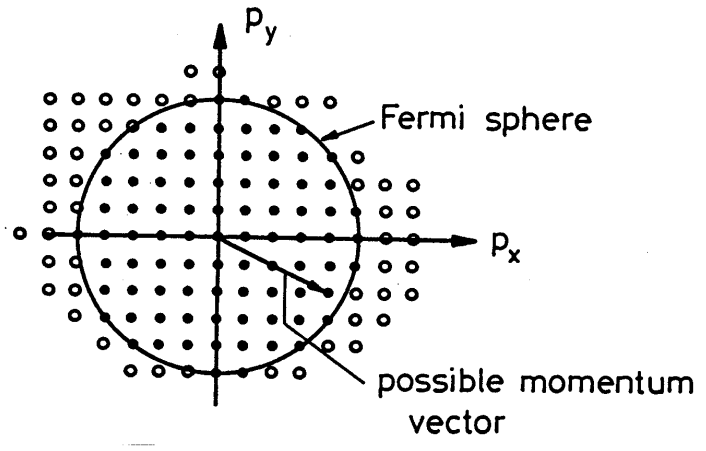

Fig. 18: The allowed states for conduction electrons in the $p_x p_y$ plane and the Fermi sphere. The occupied states are drawn as full circles, the empty states as open circles.

The quantity $\hbar = h/2\pi = 1.05 \cdot 10^{-34}$ Js $= 6.58 \cdot 10^{-15}$ eVs is Planck's constant, the most important constant in quantum theory. In order to remind the reader I will shortly sketch the derivation of these results. Consider a three-dimensional region in the metal of length $L = N\,a$, where a is the distance of neighbouring ions in the lattice and $N \gg 1$ an integer. The Schrödinger equation with potential $V = 0$ and with periodic boundary conditions $\psi(x + L, y, z) = \psi(x, y, z)$ etc. is solved by

$$\psi(x, y, z) = L^{-3/2} \exp(i(k_1 x + k_2 y + k_3 z)) \tag{22}$$

where the components of the wave vector $\vec{k}$ are given by

$$k_j = n_j \frac{2\pi}{L} \quad \text{with} \quad n_j = 0, \pm 1, \pm 2, ... \tag{23}$$

The electron momentum is $\vec{p} = \hbar\vec{k}$, the energy is $E = \hbar^2\vec{k}^2/(2m_e)$. It is useful to plot the allowed quantum states of the electrons as dots in momentum space. In Fig. 18 this is drawn for two dimensions.

In the ground state of the metal the energy levels are filled with two electrons each starting from the lowest level. The highest energy level reached is called the Fermi E_F. At temperature $T \to 0$ all states below E_F are occupied, all states above E_F are empty. The highest momentum is called the 'Fermi momentum' $p_F = \sqrt{2m_e E_F}$, the highest velocity is the Fermi velocity $v_F = p_F/m_e$ which is in the order of 10^6 m/s. In the momentum state representation, the occupied states are located inside the 'Fermi sphere' of radius p_F, the empty states are outside.

What are the consequences of the Pauli principle for electrical conduction? Let us apply an electric field $\vec{E}_0$ pointing into the negative x direction. In the time δt a free electron would gain a momentum

$$\delta p_x = eE_0\,\delta t\ . \tag{24}$$

However, most of the metal electrons are unable to accept this momentum because they do not find free states in their vicinity, only those on the right rim of the Fermi sphere have free states accessible to them and can accept the additional momentum. We see that the Pauli principle has a strong impact on electrical conduction. Heat conduction is affected in the same way because the most important carriers of thermal energy are again the electrons. An anomaly is also observed in the heat capacity of the electron gas. It

differs considerably from that of an atomic normal gas since only the electrons in a shell of thickness k_BT near the surface of the Fermi sphere can contribute. Hence the electronic specific heat per unit volume is roughly a fraction k_BT/E_F of the classical value

$$C_e \approx \frac{3}{2} n k_B \cdot \frac{k_B T}{E_F} \, .$$

This explains the linear temperature dependence of the electronic specific heat, see eq. (19).

4.12 The origin of Ohmic resistance

Before trying to understand the vanishing resistance of a superconductor we have to explain first why a normal metal has a resistance. This may appear trivial if one imagines the motion of electrons in a crystal that is densely filled with ions. Intuitively one would expect that the electrons can travel for very short distances only before hitting an ion and thereby loosing the momentum gained in the electric field. Collisions are indeed responsible for a frictional force and one can derive Ohm's law that way. What is surprising is the fact that these collisions are so rare. In an ideal crystal lattice there are no collisions whatsoever. This is impossible to understand in the particle picture, one has to treat the electrons as matter waves and solve the Schrödinger equation for a periodic potential. The resistance is nevertheless due to collisions but the collision centres are not the ions in the regular crystal lattice but only the imperfections of this lattice: impurities, lattice defects and the deviations of the metal ions from their nominal position due to thermal oscillations. The third effect dominates at room temperature and gives rise to a resistivity that is roughly proportional to T while impurities and lattice defects are responsible for the residual resistivity at low temperature ($T < 20$ K). A typical curve $\rho(T)$ is plotted in Fig. 19. In very pure copper crystals the low-temperature resistivity can become extremely small. The mean free path of the conduction electrons may be a million times larger than the distance between neighbouring ions which illustrates very well that the ions in their regular lattice positions do not act as scattering centres.

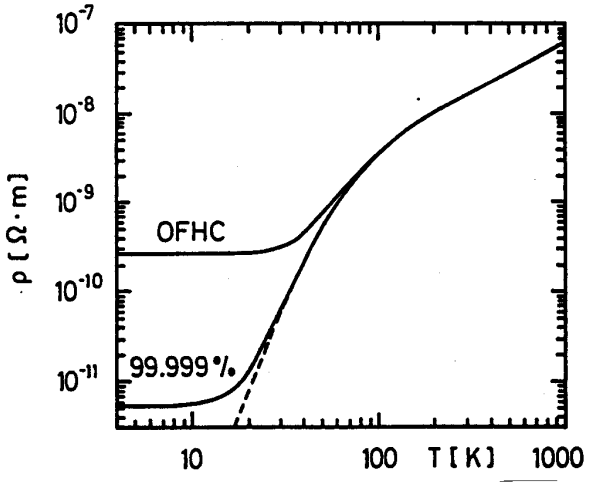

Fig. 19: Temperature dependence of the resistivity of OFHC (oxygen-free high conductivity) copper and of 99.999% pure annealed copper. Plotted as a dashed line is the calculated resistivity of copper without any impurities and lattice defects (after M.N. Wilson [17]).

4.2 Cooper pairs

We consider a metal at $T \to 0$. All states inside the Fermi sphere are filled with electrons while all states outside are empty. In 1956 Cooper studied [18] what would happen if two electrons were added

to the filled Fermi sphere with equal but opposite momenta $\vec{p}_1 = -\vec{p}_2$ whose magnitude was slightly larger than the Fermi momentum p_F (see Fig. 20). Assuming that a weak attractive force existed he was able to show that the electrons form a bound system with an energy less than twice the Fermi energy , $E_{pair} < 2E_F$. The mathematics of Cooper pair formation will be outlined in Appendix B.

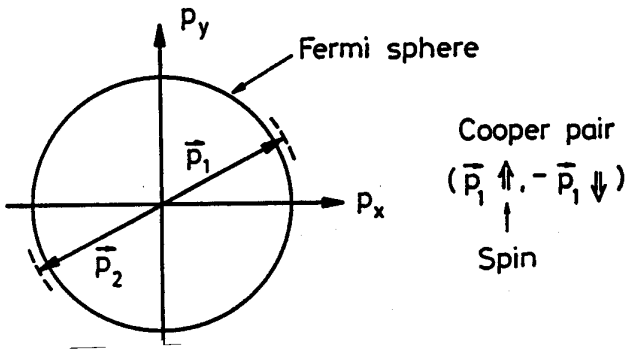

Fig. 20: A pair of electrons of opposite momenta added to the full Fermi sphere.

What could be the reason for such an attractive force? First of all one has to realize that the Coulomb repulsion between the two electrons has a very short range as it is shielded by the positive ions and the other electrons in the metal. So the attractive force must not be strong if the electrons are several lattice constants apart. Already in 1950, Fröhlich and, independently, Bardeen had suggested that a dynamical lattice polarization may create a weak attractive potential. Before going into details let us look at a familiar example of attraction caused by the deformation of a medium: a metal ball is placed on an elastic membrane and deforms the membrane such that a potential well is created. A second ball will feel this potential well and will be attracted by it. So effectively, the deformation of the elastic membrane causes an attractive force between the two balls which would otherwise not notice each other. This visualisation of a Cooper-pair is well known in the superconductivity community (see e.g. [1]) but it has the disadvantage that it is a static picture.

I prefer the following dynamic picture: suppose you are cross-country skiing in very deep snow. You will find this quite cumbersome, there is a lot of 'resistance'. Now you discover a track made by another skier, a 'Loipe', and you will immediately realize that it is much more comfortable to ski along this track than in any other direction. The Loipe picture can be adopted for our electrons. The first electron flies through the lattice and attracts the positive ions. Because of their inertia they cannot follow immediately, the shortest response time corresponds to the highest possible lattice vibration frequency. This is called the Debye frequency ω_D. The maximum lattice deformation lags behind the electron by a distance

$$d \approx v_F \frac{2\pi}{\omega_D} \approx 100 - 1000\,\mathrm{nm}\ . \tag{25}$$

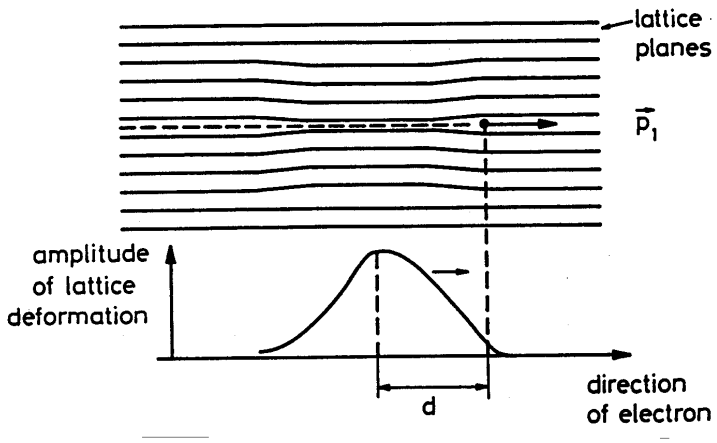

Fig. 21: Dynamical deformation of the crystal lattice caused by the passage of a fast electron. (After Ibach, L¨uth [19]).

Obviously, the lattice deformation attracts the second electron because there is an accumulation of positive charge. The attraction is strongest when the second electron moves right along the track of the first one and when it is a distance d behind it, see Fig. 21. This explains why a Cooper pair is a very extended object, the two electrons may be several 100 to 1000 lattice constants apart. For a simple cubic lattice, the lattice constant is the distance between adjacent atoms.

In the example of the cross-country skiers or the electrons in the crystal lattice, intuition suggests that the second partner should preferably have the same momentum, $\vec{p}_2 = \vec{p}_1$ although opposite momenta $\vec{p}_2 = -\vec{p}_1$ are not so bad either. Quantum theory makes a unique choice: only electrons of opposite momenta form a bound system, a Cooper pair. I don't know of any intuitive argument why this is so. (The quantum theoretical reason is the Pauli principle but there exists probably no intuitive argument why electrons obey the Pauli exclusion principle and are thus extreme individualists while other particles like the photons in a laser or the atoms in superfluid helium do just the opposite and behave as extreme conformists. One may get used to quantum theory but certain mysteries and strange feelings will remain.)

The binding energy of a Cooper pair turns out to be small, $10^{-4} - 10^{-3}$ eV, so low temperatures are needed to preserve the binding in spite of the thermal motion. According to Heisenberg's Uncertainty Principle a weak binding is equivalent to a large extension of the composite system, in this case the above-mentioned $d = 100 - 1000$ nm. As a consequence, the Cooper pairs in a superconductor overlap each other. In the space occupied by a Cooper pair there are about a million other Cooper pairs. Figure 22 gives an illustration. The situation is totally different from other composite systems like atomic nuclei or atoms which are tightly bound objects and well-separated from another. The strong overlap is an important prerequisite of the BCS theory because the Cooper pairs must change their partners frequently in order to provide a continuous binding.

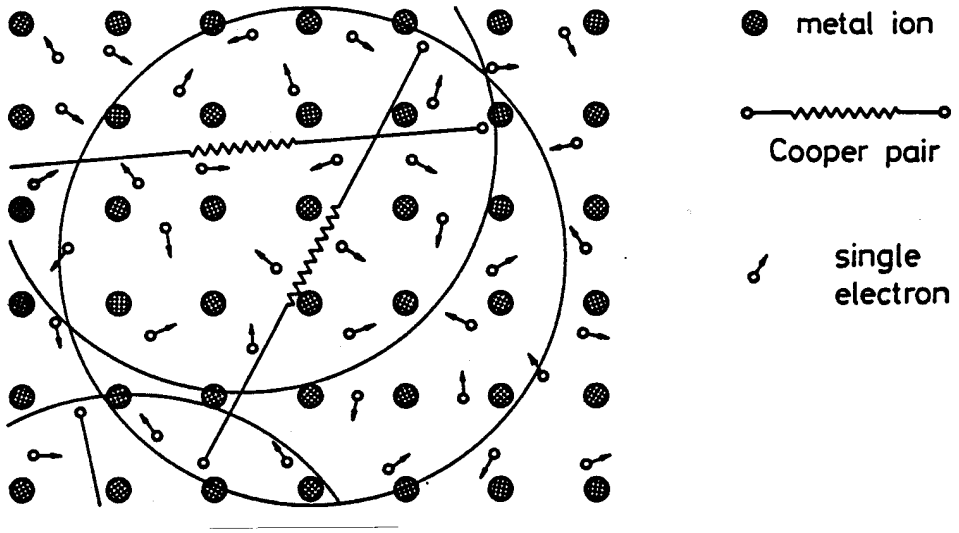

Fig. 22: Visualization of Cooper pairs and single electrons in the crystal lattice of a superconductor. (After Essmann and Tr¨auble [12]).

4.3 Elements of the BCS theory

After Cooper had proved that two electrons added to the filled Fermi sphere are able to form a bound system with an energy $E_{pair} < 2E_F$, it was immediately realized by Bardeen, Cooper and Schrieffer that also the electrons inside the Fermi sphere should be able to group themselves into pairs and thereby reduce their energy. The attractive force is provided by lattice vibrations whose quanta are the phonons. The highest possible phonon energy is

$$\hbar\omega_D = k_B\Theta_D \approx 0.01 - 0.02 \text{ eV} . \tag{26}$$

Therefore only a small fraction of the electrons can be paired via phonon exchange, namely those in a shell of thickness $\pm\hbar\omega_D$ around the Fermi energy. This is sketched in Fig. 23. The inner electrons cannot participate in the pairing because the energy transfer by the lattice is too small. One has to keep in mind though that these electrons do not contribute to normal conduction either. For vanishing electric field a Cooper pair is a loosely bound system of two electrons whose momenta are of equal magnitude but opposite direction. All Cooper pairs have therefore the same momentum $\vec{P} = 0$ and occupy exactly the same quantum state. They can be described by a macroscopic wave function Ψ in analogy with the light wave in a laser in which the photons are all in phase and have the same wavelength, direction and polarisation. The macroscopic photon wave function is the vector potential from which one can derive the electric and magnetic field vectors (see sect. 5.2).

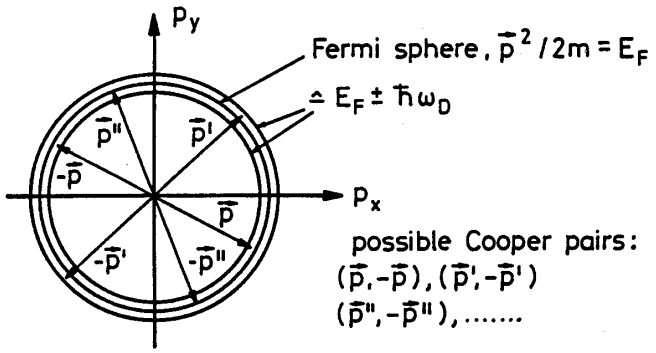

Fig. 23: Various Cooper pairs $(\vec{p}, -\vec{p})$, $(\vec{p}', -\vec{p}')$, $(\vec{p}'', -\vec{p}'')$, ... in momentum space.

The reason why Cooper pairs are allowed and even prefer to enter the same quantum state is that they behave as Bose particles with spin 0. This is no contradiction to the fact that their constituents are spin 1/2 Fermi particles. Figure 23 shows very clearly that the individual electrons forming the Cooper pairs have different momentum vectors $\vec{p}$, $\vec{p}'$, $\vec{p}''$, ... which however cancel pairwise such that the pairs have all the same momentum zero. It should be noted, though, that Cooper pairs differ considerably from other Bosons such as helium nuclei or atoms: They are not 'small' but very extended objects, they exist only in the BCS ground state and there is no excited state. An excitation is equivalent to breaking them up into single electrons.

The BCS ground state is characterized by the macroscopic wave function Ψ and a ground state energy that is separated from the energy levels of the unpaired electrons by an energy gap. In order to break up a pair an energy of 2Δ is needed, see Fig. 24.

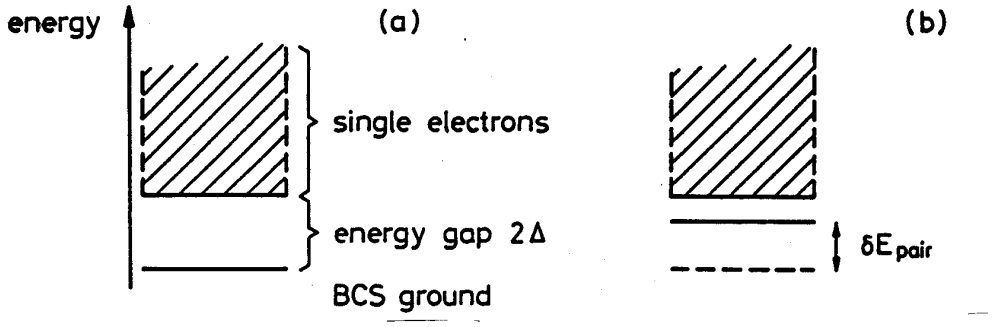

Fig. 24: (a) Energy gap between the BCS ground state and the single-electron states. (b) Reduction of energy gap in case of current fbw.

There is a certain similarity with the energy gap between the valence band and the conduction band in a semiconductor but one important difference is that the energy gap in a superconductor is not a constant but depends on temperature. For $T \to T_c$ one gets $\Delta(T) \to 0$. The BCS theory makes a quantitative prediction for the function $\Delta(T)$ which is plotted in Fig. 25 and agrees very well with experimental data.

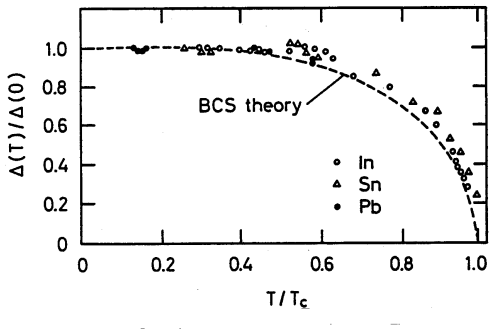

Fig. 25: Temperature dependence of the energy gap according to the BCS theory and comparison with experimental data.

One of the fundamental formulae of the BCS theory is the relation between the energy gap $\Delta(0)$ at $T = 0$, the Debye frequency ω_D and the electron-lattice interaction potential V_0:

$$\Delta(0) = 2\hbar\omega_D \exp\left(-\frac{1}{V_0 \mathcal{N}(E_F)}\right) . \tag{27}$$

Here $\mathcal{N}(E_F)$ is the density of single-electron states of a given spin orientation at $E = E_F$ (the other spin orientation is not counted because a Cooper pair consists of two electrons with opposite spin). Although the interaction potential V_0 is assumed to be weak, one of the most striking observations is that the exponential function cannot be expanded in a Taylor series around $V_0 = 0$ because all coefficients vanish identically. This implies that Eq. (27) is a truely non-perturbative result. The fact that superconductivity cannot be derived from normal conductivity by introducing a 'small' interaction potential and applying perturbation theory (which is the usual method for treating problems of atomic, nuclear and solid state physics that have no analytical solution) explains why it took so many decades to find the correct theory. The critical temperature is given by a similar expression

$$k_B T_c = 1.14\,\hbar\omega_D \exp\left(-\frac{1}{V_0 \mathcal{N}(E_F)}\right) . \tag{28}$$

Combining the two equations we arrive at a relation between the energy gap and the critical temperature which does not contain the unknown interaction potential

$$\Delta(0) = 1.76\, k_B T_c . \tag{29}$$

The following table shows that this remarkable prediction is fulfilled rather well.

element	Sn	In	Tl	Ta	Nb	Hg	Pb
$\Delta(0)/k_B T_c$	1.75	1.8	1.8	1.75	1.75	2.3	2.15

In the BCS theory the underlying mechanism of superconductivity is the attractive force between pairs of electrons that is provided by lattice vibrations. It is of course highly desirable to find experimental support of this basic hypothesis. According to Eq. (28) the critical temperature is proportional to the Debye frequency which in turn is inversely proportional to the square root of the atomic mass M:

$$T_c \propto \omega_D \propto 1/\sqrt{M} .$$

If one produces samples from different isotopes of a superconducting element one can check this relation. Figure 26 shows T_c measurements on tin isotopes. The predicted $1/\sqrt{M}$ law is very well obeyed.

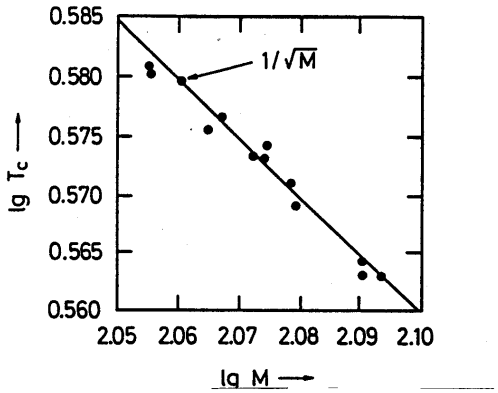

Fig. 26: The critical temperature of various tin isotopes.

4.4 Supercurrent and critical current

The most important task of a theory of superconductivity is of course to explain the vanishing resistance. We have seen in sect. 4.1 that the electrical resistance in normal metals is caused by scattering processes so the question is why Cooper pairs do not suffer from scattering while unpaired electrons do. To start a current in the superconductor, let us apply an electric field $\vec{E}_0$ for a short time δt. Both electrons of a Cooper pair receive an additional momentum $\delta\vec{p} = -e\vec{E}_0\,\delta t$ so after the action of the field all Cooper pairs have the same non-vanishing momentum

$$\vec{P} = \hbar\vec{K} = -2\vec{E}_0\,\delta t\ .$$

Associated with this coherent motion of the Cooper pairs is a supercurrent density

$$\vec{J}_s = -n_c\frac{e\hbar}{m_e}\vec{K}\ . \tag{30}$$

Here n_c is the Cooper-pair density. It can be shown (see e.g. Ibach, Lüth [19]) that the Cooper-pair wave function with a current flowing is simply obtained by multiplying the wave function at rest with the phase factor $\exp(i\vec{K}\cdot\vec{R})$ where $\vec{R} = (\vec{r}_1 + \vec{r}_2)/2$ is the coordinate of the centre of gravity of the two electrons. Moreover the electron-lattice interaction potential is not modified by the current flow. So all equations of the BCS theory remain applicable and there will remain an energy gap provided the kinetic-energy gain $\delta E_{\rm pair}$ of the Cooper pair is less than 2Δ, see Fig. 24b. It is this remaining energy gap which prevents scattering. As we have seen there are two types of scattering centres: impurities and thermal lattice vibrations. Cooper pairs can only scatter when they gain sufficient energy to cross the energy gap and are then broken up into single electrons. An impurity is a fixed heavy target and scattering cannot increase the energy of the electrons of the pair, therefore impurity scattering is prohibited for the Cooper pairs. Scattering on thermal lattice vibrations is negligible as long as the average thermal energy is smaller than the energy gap (that means as long as the temperature is less than the critical temperature for the given current density). So we arrive at the conclusion that there is resistance-free current transport provided there is still an energy gap present ($2\Delta - \delta E_{pair} > 0$) and the temperature is sufficiently low ($T < T_c(J_s)$).

The supercurrent density is limited by the condition that the energy gain $\delta E_{\rm pair}$ must be less than the energy gap. This leads to the concept of the *critical current density* J_c. The energy of the Cooper pair is, after application of the electric field,

$$E_{pair} = \frac{1}{2m_e}\left((\vec{p}+\vec{P}/2)^2 + (-\vec{p}+\vec{P}/2)^2\right) = \frac{\vec{p}^{\,2}}{m_e} + \delta E_{pair}$$

with $\delta E_{pair} \approx p_F P/m_e$. From the condition $\delta E_{\rm pair} \leq 2\Delta$ we get

$$J_s \leq J_c \approx 2e\, n_c\, \Delta/p_F\ . \tag{31}$$

Coupled to a maximum value of the current density is the existence of a critical magnetic field. The current flowing in a long wire of type I superconductor is confined to a surface layer of thickness λ_L, see Fig. 6c. The maximum permissible current density J_c is related to the critical field:

$$H_c(T) = \lambda_L\, J_c(T) \approx \lambda_L\, 2en_c\, \Delta(T)/p_F\ . \tag{32}$$

The temperature dependence of the critical field is caused by the temperature dependence of the gap energy.

The above considerations on resistance-free current flow may appear a bit formal so I would like to give a more familiar example where an energy gap prevents 'resistance' in a generalized sense. We compare crystals of diamond and silicon. Diamond is transparent to visible light, silicon is not. So silicon represents a 'resistance' to light. Why is this so? Both substances have exactly the same crystal structure, namely the 'diamond lattice' that is composed of two face-centred cubic lattices which are displaced by one quarter along the spatial diagonal. The difference is that diamond is built up from carbon atoms and is an electrical insulator while a silicon crystal is a semiconductor. In the band theory of solids there is an energy gap E_g between the valence band and the conduction band. The gap energy is around 7 eV for diamond and 1 eV for silicon. Visible light has a quantum energy of about 2.5 eV. A photon impinging on a silicon crystal can lift an electron from the valence band to the conduction band and is thereby absorbed. The same photon impinging on diamond is unable to supply the required energy of 7 eV, so this photon simply passes the crystal without absorption: diamond has no 'resistance' for light. (Quantum conditions of this kind have already been known in the Stone Age. If hunters wanted to catch an antelope that could jump 2 m high, they would dig a hole 4 m deep and then the animal could never get out because being able to jump 2 m in two successive attempts is useless for overcoming the 4 m. The essential feature of a quantum process, namely that the energy gap has to be bridged in a single event, is already apparent in this trivial example).

Finally, I want to give an example for frictionless current flow. The hexagonal benzene molecule C_6H_6 is formed by covalent binding and contains 24 electrons which are localised in σ bonds in the plane of the molecule and 6 electrons in π bonds below and above this plane. The π electrons can move freely around the ring. By a time-varying magnetic field a ring current is induced (benzene is a diamagnetic molecule) which will run forever unless the magnetic field is changed. This resembles closely the operation of a superconducting ring in the persistent mode (see Fig. 27).

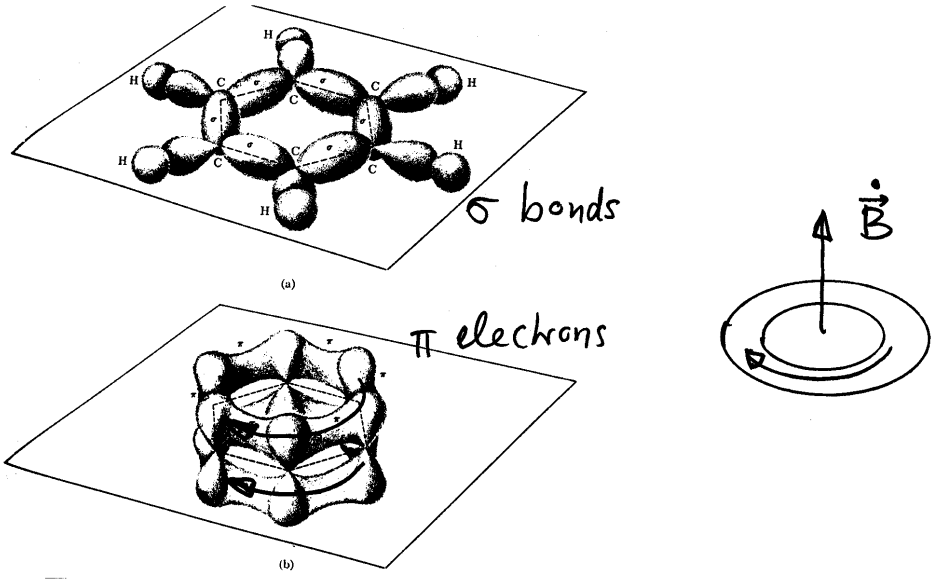

Fig. 27: Persistent ring currents in a benzene molecule and in a superconducting ring which have been induced by a rising fi eld B_z.

5. QUANTISATION OF MAGNETIC FLUX

Several important superconductor properties, in particular the magnetic flux quantisation, can only be explained by studying the magnetic vector potential and its impact on the so-called 'canonical momentum' of the charge carriers. Since this may not be a familiar concept I will spend some time to discuss the basic ideas and the supporting experiments which are beautiful examples of quantum interference phenomena.

5.1 The vector potential in electrodynamics

In classical electrodynamics it is often a matter of convenience to express the magnetic field as the curl (rotation) of a vector potential

$$\vec{B} = \vec{\nabla} \times \vec{A} \, .$$

The magnetic flux through an area F can be computed from the line integral of $\vec{A}$ along the rim of F by using Stoke's theorem:

$$\Phi_{mag} = \int \int \vec{B} \cdot d\vec{F} = \oint \vec{A} \cdot \vec{ds} \, . \tag{33}$$

We apply this to the solenoidal coil sketched in Fig. 28.

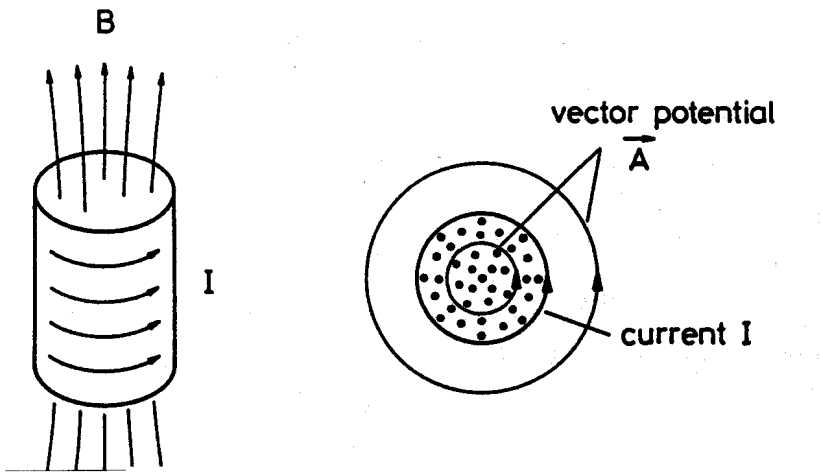

Fig. 28: Magnetic fi eld and vector potential of a solenoid.

The magnetic field has a constant value $B = B_0$ inside the solenoid and vanishes outside if we the length of the coil is much larger than its radius R. The vector potential has only an azimuthal component and can be computed using Eq. (33):

$$A_\theta(r) = \begin{cases} \frac{1}{2} B_0 \cdot r & \text{for } r < R \\ \frac{1}{2} B_0 \dfrac{R^2}{r} & \text{for } r > R \end{cases} .$$

Evaluating $\vec{B} = \vec{\nabla} \times \vec{A}$ in cylindrical coordinates gives the expected result

$$B_z(r) = \begin{cases} B_0 & \text{for } r < R \\ 0 & \text{for } r > R \end{cases} .$$

What do we learn from this example?
(a) The vector potential is parallel to the current but perpendicular to the magnetic field.
(b) There are regions in space where the vector potential is non-zero while the magnetic field vanishes. Here it is the region $r > R$. A circular contour of radius $r > R$ includes magnetic flux, namely $B_0 \pi R^2$ for all $r > R$, so $\vec{A}$ must be non-zero, although $\vec{B} = 0$.

The vector potential is not uniquely defined. A new potential $\vec{A}' = \vec{A} + \vec{\nabla}\chi$ with an arbitrary scalar function $\chi(x, y, z)$ leaves the magnetic field $\vec{B}$ invariant because the curl of a gradient vanishes identically. For this reason it is often said that the vector potential is just a useful mathematical quantity without physical significance of its own. In quantum theory this point of view is entirely wrong, the vector potential is of much deeper physical relevance than the magnetic field.

5.2 The vector potential in quantum theory

In quantum theory the vector potential is a quantity of fundamental importance:
(1) $\vec{A}$ is the wave function of the photons,
(2) in an electromagnetic field the wavelength of a charged particle is modified by the vector potential.
For the application in superconductivity we are interested in the second aspect. The *de Broglie relation* states that the wavelength we have to attribute to a particle is Planck's constant divided by the particle

momentum

$$\lambda = \frac{2\pi\hbar}{p} \ . \tag{34}$$

For a free particle one has to insert $p = mv$. It turns out that in the presence of an electromagnetic field this is no longer correct, instead one has to replace the mechanical momentum $m\vec{v}$ by the so-called 'canonical momentum'

$$\vec{p} = m\vec{v} + q\vec{A} \tag{35}$$

where q is the charge of the particle ($q = -e$ for an electron). The wavelength is then

$$\lambda = \frac{2\pi\hbar}{mv + qA} \ .$$

If one moves by a distance Δx, the phase φ of the electron wave function changes in free space by the amount

$$\Delta\varphi = \frac{2\pi}{\lambda}\Delta x = \frac{1}{\hbar} m_e \vec{v} \cdot \vec{\Delta x} \ .$$

In an electromagnetic field there is an additional phase change

$$\Delta\varphi' = -\frac{e}{\hbar}\vec{A} \cdot \vec{\Delta x} \ .$$

This is called the *Aharonov-Bohm effect* after the theoreticians who predicted the phenomenon [20]. The phase shift should be observable in a double-slit experiment as sketched in Fig. 29. An electron beam is split into two coherent sub-beams and a tiny solenoid coil is placed between these beams. The sub-beam 1 travels antiparallel to $\vec{A}$, beam 2 parallel to $\vec{A}$. So the two sub-beams gain a phase difference

$$\delta\varphi = \delta\varphi_0 + \frac{e}{\hbar}\oint \vec{A} \cdot \vec{ds} = \delta\varphi_0 + \frac{e}{\hbar}\Phi_{mag} \ . \tag{36}$$

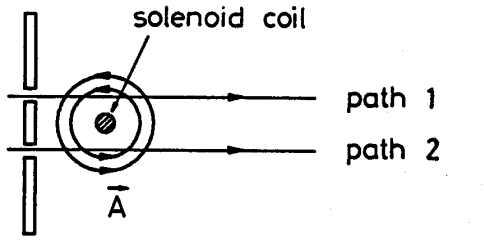

Fig. 29: Schematic arrangement for observing the phase shift due to a vector potential.

Here $\delta\varphi_0$ is the phase difference for current 0 in the coil. The Aharonov-Bohm effect was verified in a beautiful experiment by Möllenstedt and Bayh in Tübingen [21]. The experimental setup and the result of the measurements are shown in Fig. 30. An electron beam is split by a metalized quartz fibre on negative potential which acts like an optical bi-prism. Two more fibres bring the two beams to interference on a photographic film. Very sharp interference fringes are observed. Between the sub-beams is a 14 μm–diameter coil wound from 4 μm thick tungsten wire. The current in this coil is first zero, then increased linearly with time and after that kept constant. The film recording the interference pattern is moved in the vertical direction. Thereby the moving fringes are depicted as inclined lines. The observed shifts are in quantitative agreement with the prediction of Eq. (36).

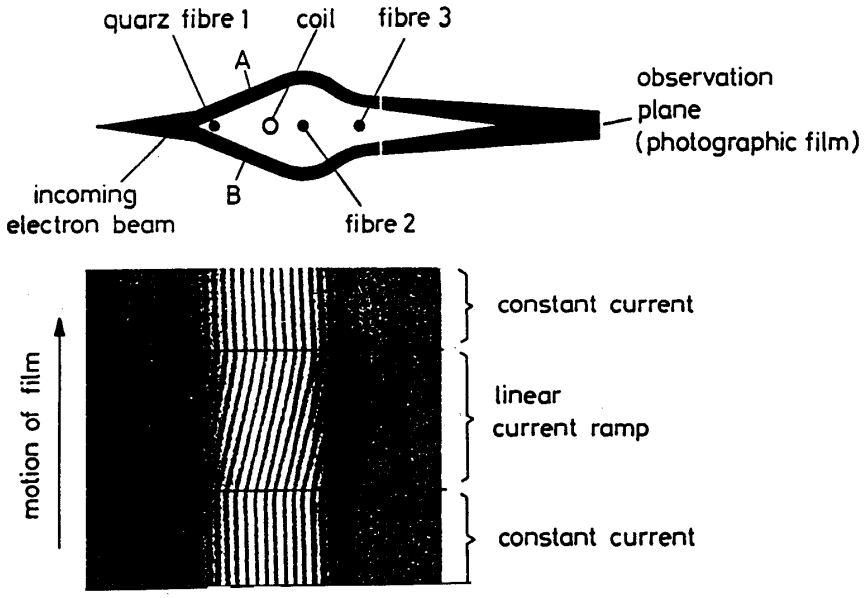

Fig. 30: Sketch of the M¨ollenstedt-Bayh experiment and observed interference pattern.

An interesting special case is the phase shift $\delta\varphi = \pi$ that interchanges bright and dark fringes. According to Eq. (36) this requires a magnetic flux

$$\Phi_{mag} = \pi\frac{\hbar}{e} = \frac{h}{2e}$$

which turns out to be identical to the elementary flux quantum in superconductors, see sect. 5.3. In the Möllenstedt experiment however, continuous phase shifts much smaller than π are visible, so the magnetic flux through the normal-conducting tungsten coil is not quantised (there is also no theoretical reason for flux quantisation in normal conductors).

Although the magnetic field is very small outside the solenoid, and the observed phase shifts are in quantitative agreement with the expectation based on the vector potential, there have nevertheless been sceptics who tried to attribute the observed effects to some stray magnetic field. To exclude any such explanation a new version of the experiment has recently been carried out by Tonomura et al. [22] making use of electron holography (Fig. 31). A parallel electron beam is imaged by an electron microscope lens on a photographic plate. To create a holographic pattern the object is placed in the upper half of the beam while the lower half serves as a reference beam. A metalized quartz fibre (the bi-prism) brings the two-part beam to an overlap on the plate. The magnetic field is provided by a permanently magnetised ring of with a few μm diameter. The magnet is enclosed in niobium and cooled by liquid helium so the magnetic field is totally confined. The vector potential, however, is not shielded by the superconductor. The field lines of $\vec{B}$ and $\vec{A}$ are also drawn in the figure. The holographic image shows again a very clear interference pattern and a shift of the dark line in the opening of the ring which is caused by the vector potential. This experiment demonstrates beyond any doubt that it is the vector potential and not the magnetic field which influences the wavelength of the electron and the interference pattern.

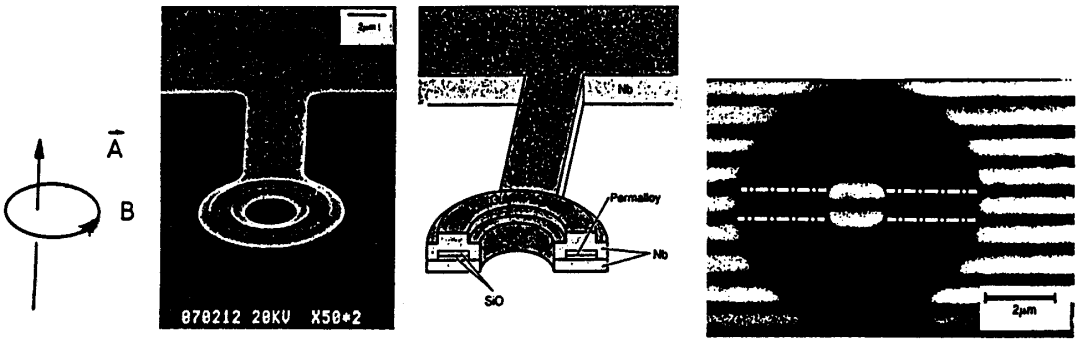

Fig. 31: Observation of Aharonov-Bohm effect using electron holography (after Tonomura [22]). The permanent toroidal magnet, encapsuled in superconducting niobium, and the observed interference fringes are shown.

5.3 Flux quantisation

The Meissner-Ochsenfeld effect excludes magnetic field from the bulk of a type I superconductor. An interesting situation arises if one exposes a superconducting ring to a magnetic field. Then one can obtain a trapped flux, threading the hole of the ring as shown in Fig. 32. Both the London and the BCS theory make the surprising prediction that the flux through the hole cannot assume arbitrary values but is quantised, i.e. that it is an integer multiple of an elementary flux quantum

$$\Phi_{\rm mag} = n\,\Phi_0\,, \quad n = 0, 1, 2, \ldots \tag{37}$$

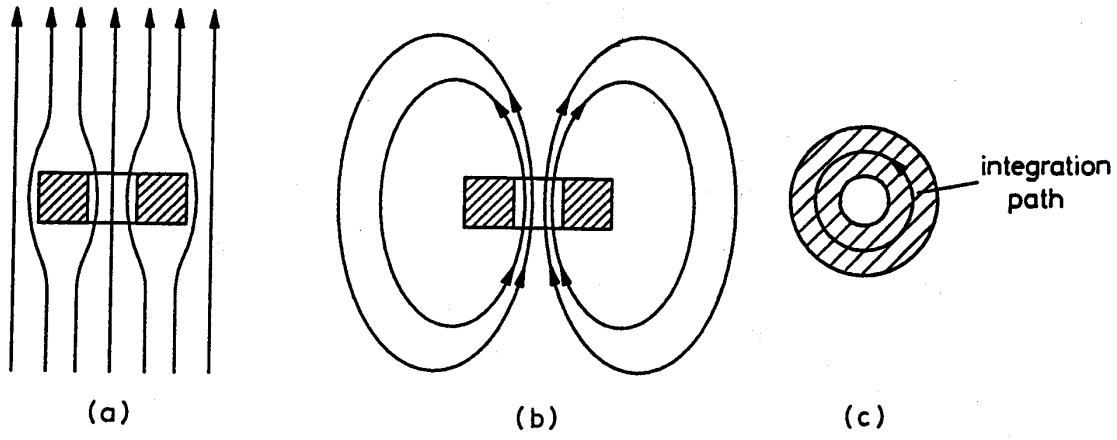

Fig. 32: Trapping of magnetic flux in a ring. First the normal-conducting ring ($T > T_c$) is placed in a magnetic field, then it is cooled down (a) and finally the field is switched off (b). The integration path is shown in part (c).

The flux quantum is Planck's constant divided by the charge of the supercurrent carriers. The BCS flux quantum is thus

$$\Phi_0 = \frac{h}{2e} \tag{38}$$

while the London flux quantum is twice as big because the charge carriers in the London theory are single electrons.

5.31 Derivation of flux quantisation

The Cooper-pair wave function in the ring can be written as

$$\Psi = \sqrt{n_c}\exp(i\varphi) \ .$$

The density of Cooper pairs is denoted as n_c. The phase $\varphi = \varphi(s)$ has to change by $n \cdot 2\pi$ when going once around the ring since Ψ must be a single-valued wave function. We choose a circular path in the bulk of the ring (Fig. 31c). Then

$$\oint \frac{d\varphi}{ds} ds = n \cdot 2\pi \ .$$

In other words: the circumference must be an integer number of wavelengths. In the bulk there is no current allowed so the Cooper-pair velocity must be zero, $\vec{v} = 0$. Therefore the integrand is

$$\frac{d\varphi}{ds} ds = \frac{q}{\hbar}\vec{A} \cdot \vec{ds} \ .$$

Using Eq. (33) we see that the magnetic flux enclosed by the circular path is

$$\Phi_{mag} = \oint \vec{A} \cdot \vec{ds} = \frac{\hbar}{q} \cdot n \cdot 2\pi = n \cdot \Phi_0 \quad \Rightarrow \quad \Phi_0 = \frac{2\pi\hbar}{q} \ . \tag{39}$$

In the BCS theory we have $q = -2e$ and hence $\Phi_0 = h/(2e)$.

5.32 Experimental verification of flux quantisation

In 1961 two experiments on flux quantisation were carried out almost simultaneously, by Doll and Näbauer [23] in München and by Deaver and Fairbank [24] in Stanford. I describe the Doll-Näbauer experiment as it yielded the best evidence. The setup and the results are shown in Fig. 33. The superconducting ring is here a lead tube prepared by evaporation of lead on a 10 μm–thick quartz cylinder which is then suspended by a torsion fibre. Magnetic flux is captured in the tube by exposing the warm tube to a 'magnetising field' B_{mag} parallel to the axis, cooling down and switching off the field. Then a transverse oscillating field B_{osc} is applied to induce forced oscillations which are observed by light reflection from a small mirror. The resonant amplitude A_{res} is proportional to the magnetic moment of the tube and hence to the captured magnetic flux. Without flux quantisation the relation between resonant amplitude and magnetising field should be linear. Instead one observes a very pronounced stair-case structure which can be uniquely related to frozen-in fluxes of 0, 1 or 2 flux quanta. Both experiments proved that the magnetic flux quantum is $h/2e$ and not h/e and thus gave strong support for the Cooper-pair hypothesis.

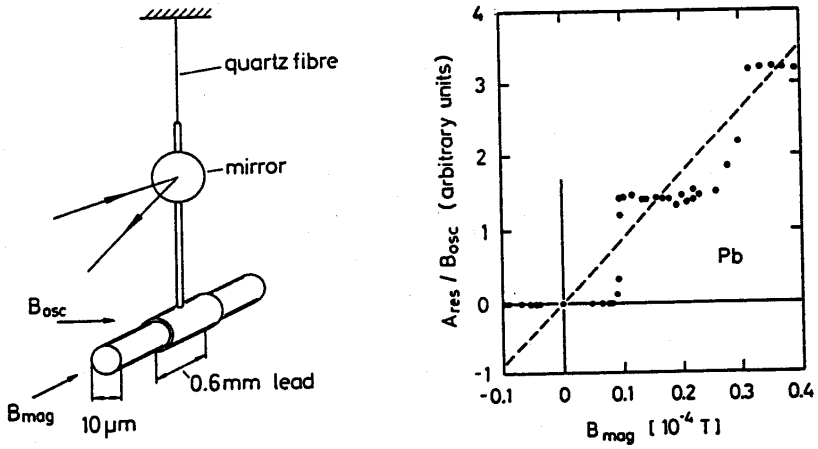

Fig. 33: Observation of flux quantisation [23].

The BCS theory is not directly applicable to high-T_c superconductors[2] which are basically two-dimensional superconductors. In Fig. 34 the flux through a $YBa_2Cu_3O_7$ ring with a weak joint is shown. Flux jumps due to external field variations occur in multiples of $h/2e$ which is an indication that some kind of Cooper pairing is also responsible for the superconductivity in these materials.

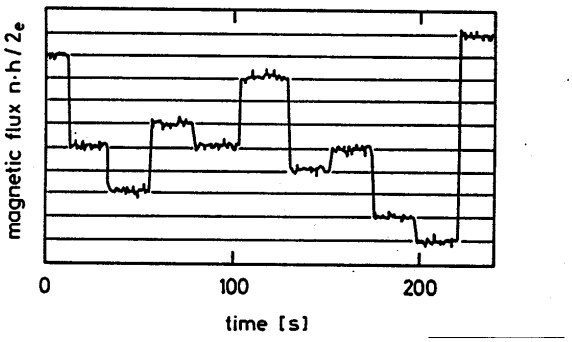

Fig. 34: Flux through an $YBa_2Cu_3O_7$ ring with a weak link [26].

In another interesting experiment a lead strip was bent into ring shape and closed via an intermediate $YBa_2Cu_3O_7$ piece. It was possible to induce a persistent ring current in this combined system of a low-T_c and a high-T_c superconductor.

5.4 Fluxoid pattern in type II superconductors

Abrikosov predicted that a magnetic field penetrates a type II superconductor in the form of flux tubes or fluxoids, each containing a single elementary quantum Φ_0, which arrange themselves in a quadratic or triangular pattern to minimize the potential energy related to the mutual repulsion of the flux tubes. A schematic cross section of a fluxoid is presented in Fig. 35. The magnetic field lines are surrounded by

[2]For a review of high-T_c superconductors see ref. [25] and the lectures by R. Fluekiger.

a super-current vortex. The Cooper-pair density drops to zero at the centre of the vortex, so the core of a flux tube is normal-conducting.

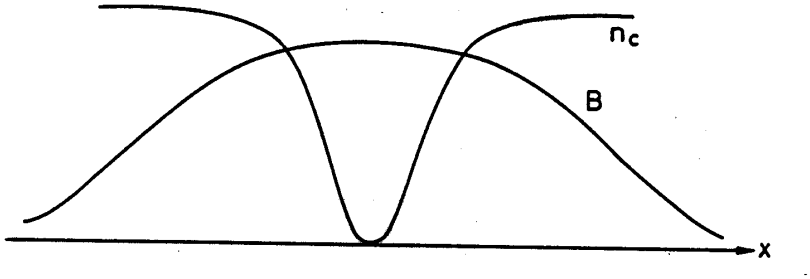

Fig. 35: Schematic cross section of a fluxoid.

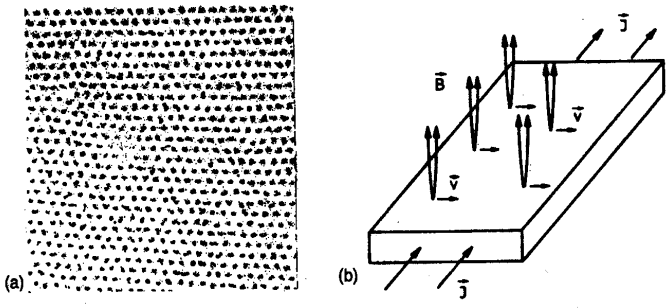

Fig. 36: (a) Fluxoid pattern in niobium (courtesy U. Essmann). The distance between adjacent flux tubes is 0.2 μm. (b) Fluxoid motion in a current-carrying type II superconductor.

The area occupied by a fluxoid is roughly given by $\pi\xi^2$ where ξ is the coherence length. An estimate of the upper critical field is derived from the condition that the fluxoids start touching each other:

$$B_{c2} \approx \frac{\Phi_0}{2\pi\xi^2} \; . \tag{40}$$

An important experimental step was the direct observation of the fluxoid pattern. Essmann and Träuble [12] developed a 'decoration' technique for this purpose. A superconductor sample was cooled by a liquid helium bath with the surface sticking out of the liquid. Iron was evaporated at some distance from the superconductor, and in the helium gas atmosphere the iron atoms agglomerated to tiny crystals (about 20 nm) that were attracted by the magnetic field lines and stuck to the sample surface where the fluxoids emerged. After warming up, a thin film was sprayed on the surface to allow the iron crystals to be removed for subsequent observation in an electron microscope. The photograph in Fig. 36a shows indeed the perfect triangular pattern predicted by Abrikosov. Similar pictures have been recently obtained with high-temperature superconductors. The electron holography setup mentioned in the last section permits direct visualization of the magnetic flux lines. Figure 37 is an impressive example of the capabilities of this advanced method.

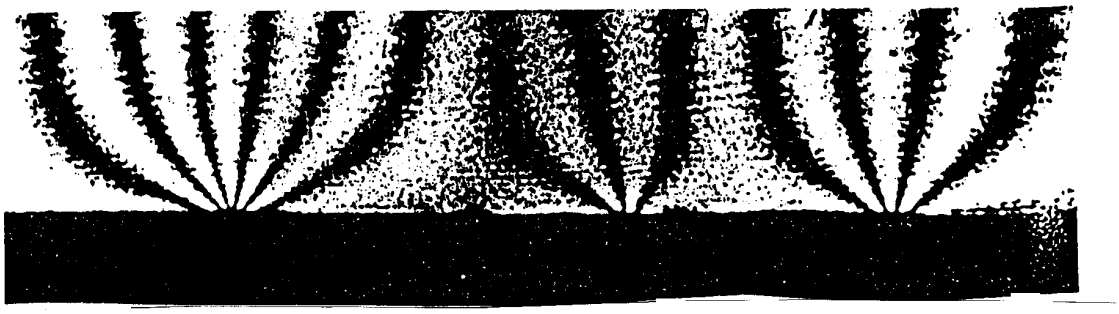

Fig. 37: Holographic image of the magnetic flux lines through a thin lead plate [22].

6. Hard Superconductors

6.1 Flux flow resistance and flux pinning

For application in accelerator magnets a superconducting wire must be able to carry a large current in the presence of a field in the 5 – 10 Tesla range. Type I superconductors are definitely ruled out because their critical field is less than a few tenths of a Tesla and their current-carrying capacity is very small since the current is restricted to a thin surface layer (compare Fig. 6). Type II conductors appear quite appropriate on first sight: they have a large upper critical field and high currents are permitted to flow in the bulk material. Still there is a problem, called *flux flow resistance*. If a current flows through an ideal type II superconductor which is exposed to a magnetic field one observes heat generation. The current density $\vec{J}$ exerts a Lorentz force on the flux lines. The force per unit volume is

$$\vec{F} = \vec{J} \times \vec{B} \; .$$

The flux lines begin to move through the specimen in a direction perpendicular to the current and to the field (Fig. 36b). This is a viscous motion ($\vec{v} \propto \vec{F}$) and leads to heat generation. So although the current itself flows without dissipation the sample acts as if it had an Ohmic resistance. The statement is even formally correct. The moving fluxoids represent a moving magnetic field. According to Special Relativity this is equivalent to an electric field

$$\vec{E}_{equiv} = \frac{1}{c^2} \vec{B} \times \vec{v} \; .$$

It is easy to see that $\vec{E}_{equiv}$ and $\vec{J}$ point in the same direction just like in a normal resistor. Flux flow resistance was studied experimentally by Kim and co-workers [28].

To obtain useful wires for magnet coils the flux motion has to be inhibited. The standard method is to capture them at *pinning centres*. The most important pinning centres in niobium-titanium are normal-conducting Ti precipitates with a size in the 10 nm range. Flux pinning is discussed in detail in M.N. Wilson's lectures at this school. A type II superconductor with strong pinning is called a *hard superconductor*. Hard superconductors are very well suited for high-field magnets, they permit dissipationless current flow in high magnetic fields. There is a penalty, however: these conductors exhibit a strong magnetic hysteresis which is the origin of the very annoying 'persistent-current' multipoles in superconducting accelerator magnets.

6.2 Magnetisation of a hard superconductor

A type I superconductor shows a reversible response[3] to a varying external magnetic field H. The magnetization is given by the linear relation $\vec{M}(\vec{H}) = -\vec{H}$ for $0 < H < H_c$ and then drops to zero, see Fig. 10. An ideal type II conductor without any flux pinning should also react reversibly. A hard superconductor, on the other hand, is only reversible in the Meissner phase because then no magnetic field enters the bulk, so no flux pinning can happen. If the field is raised beyond H_{c1} magnetic flux enters the sample and is captured at pinning centres. When the field is reduced again these flux lines remain bound and the specimen keeps a frozen-in magnetisation even for vanishing external field. One has to invert the field polarity to achieve $M = 0$ but the initial state ($H = 0$ and no captured flux in the bulk material) can only be recovered by warming up the specimen to destroy superconductivity and release all pinned flux quanta, and by cooling down again.

A typical hysteresis curve is shown in Fig. 38a. There is a close resemblence with the hysteresis in iron except for the sign: the magnetisation in a superconductor is opposed to the magnetising field because the underlying physical process is diamagnetism. In an accelerator the field is usually not inverted and then the hysteresis has the shape plotted in Fig. 38b.

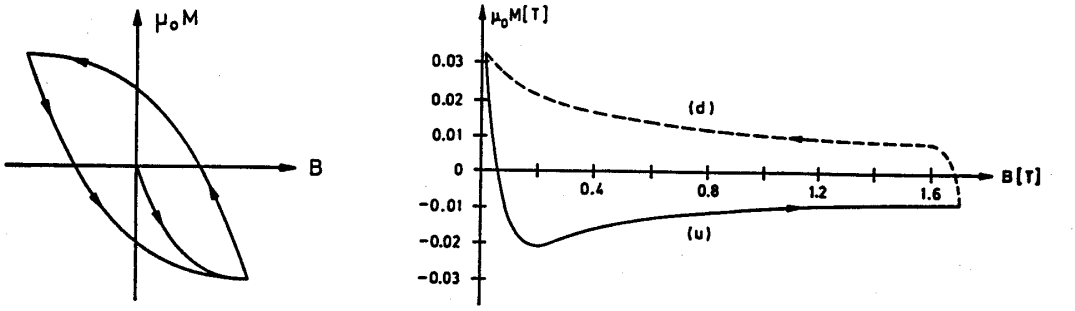

Fig. 38: (a) Magnetic hysteresis of a hard superconductor. (b) Magnetisation hysteresis for the field cycle of accelerator magnets.

Detailed studies on superconductor magnetisation were performed in the HERA dipoles. The sextupole component is a good measure of M. Immediately after cooldown a dipole was excited to low fields. In Fig. 39 the sextupole field B_3 at a distance of 25 mm from the dipole axis is plotted as a function of the dipole field $B_1 = \mu_0 H_1$ on the axis. One can see that the sextupole is a reversible function of B_1 up to about 25 mT (the lower critical field of NbTi is somewhat smaller, around 15 mT, but in most parts of the coil the local field is less than the value B_1 on the axis). The superconducting cable is therefore in the Meissner phase. Increasing B_1 to 50 mT already leads to a slight hysteresis so a certain amount of magnetic flux enters the NbTi filaments and is captured there.

[3]This statement applies only for long cylindral or elliptical samples oriented parallel to the field.

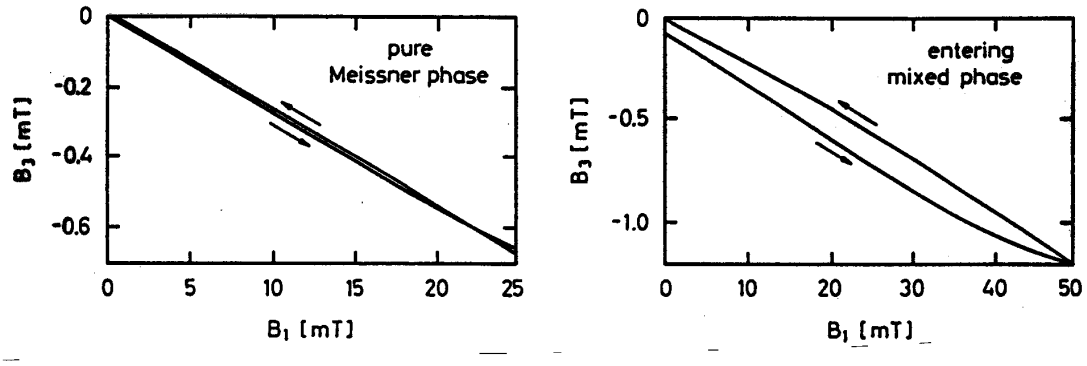

Fig. 39: Sextupole field in a HERA dipole in the Meissner phase and slightly above.

With increasing field the hysteresis widens more and more and is eventually nearly symmetric to the horizontal axis. The sextupole hysteresis observed in the standard field cycle at HERA is plotted in Fig. 40a. A similar curve is obtained for the 12-pole in the quadrupoles.

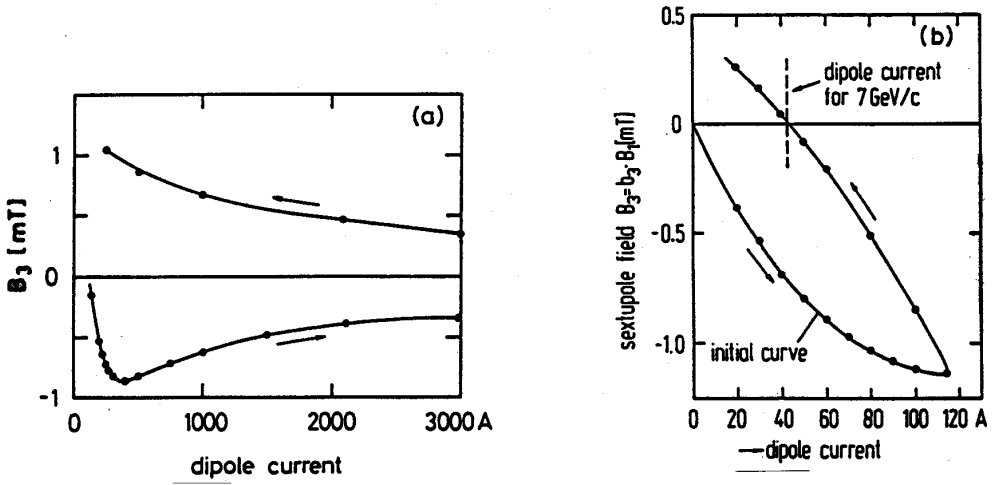

Fig. 40: (a) The sextupole component in the HERA dipoles for the standard field cycle 4.7 T → 0.05 T → 4.7 T. (b) Sextupole field for the first beam test with positrons of 7 GeV.

Only in a 'virgin' magnet, that is right after cool-down, is there the chance to influence the width of the hysteresis curve. This fact was used to advantage during the commissioning of the HERA proton storage ring. The first beam test was made with positrons of only 7 GeV since the nominal 40 GeV protons were not yet available. At the corresponding dipole field of 70 mT (coil current 42.5 A) the persistent-current sextupole component would have been two orders of magnitude larger than tolerable if the standard field cycle had been used. To eliminate the sextupole, all magnets were warmed to 20 K to extinguish any previous superconductor magnetisation and cooled back to 4.4 K. Then the current loop 0 → 112 A → 42.5 A was performed which resulted in an almost vanishing sextupole (see Fig. 40b). A similar procedure was used in the first run with 40 GeV protons, this time with the loop 0 → 314 A → 245 A. The measured chromaticity indeed proved an almost perfect sextupole cancellation.

For the routine operation of HERA these procedures are of course not applicable because they require a warm-up of the whole ring. Instead, sextupole correction coils must be used to compensate the unwanted field distortions.

6.3 Flux creep

The pinning centres prevent flux flow in hard superconductors but some small *flux creep* effects remain. At finite temperatures, even as low as 4 K, a few of the flux quanta may be released from their pinning locations by thermal energy and then move out of the specimen thereby reducing the magnetisation. The first flux creep experiment was carried out by Kim et al. [29] using a small NbZr tube. If one plots the internal field at the centre of the tube as a function of the external field the well-known hysteresis curve is obtained in which one can distinguish the shielding and the trapping branch, see Fig. 41a. Kim and co-workers realized that on the trapping branch the internal field exhibited a slow logarithmic decrease with time while on the shielding branch a similar increase was seen (Fig. 41b).

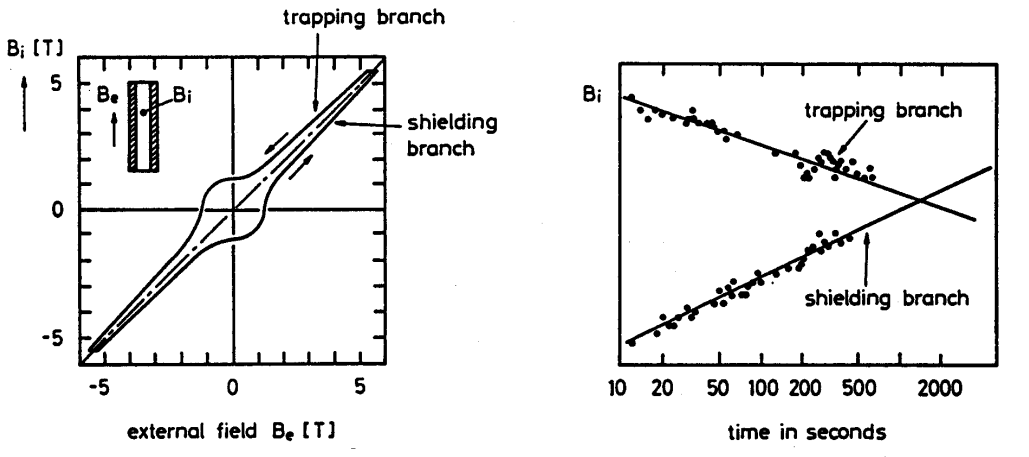

Fig. 41: (a) Hysteresis of the internal field in a tube of hard superconductor. (b) Time dependence of the internal field on the trapping and the shielding branch [29].

A logarithmic time dependence is something rather unusual. In an electrical circuit with inductive and resistive components the current decays exponentially like $\exp(-t/\tau)$ with a time constant $\tau = L/R$. A theoretical model for thermally activated flux creep was proposed by Anderson [30]. The pinning centres are represented by potential wells of average depth U_0 and width a in which bundles of flux quanta with an average flux $\Phi_{av} = n\Phi_0$ are captured. At zero current the probability that flux leaves a potential well is proportional to the Boltzmann factor

$$P_0 \propto \exp(-U_0/k_BT) \; .$$

When the superconductor carries a current density J the potential acquires a slope proportional to the force density $F \propto \Phi_{av}J$. This slope reduces the effective potential well depth to $U = U_0 - \Delta U$with $\Delta U \approx \Phi_{av}Jal$, see Fig. 42. Here l is the length of the flux bundle. The probability for flux escape increases

$$P = P_0 \exp(+\Delta U/k_BT) \; .$$

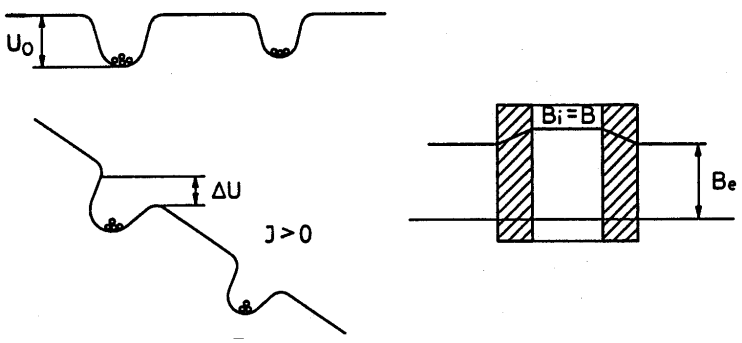

Fig. 42: Sketch of the pinning potential without and with current fbw and fi eld profi le across the NbZr tube.

We consider now the tube in the Kim experiment at a high external field B_{ext} on the trapping branch of the hysteresis curve. The internal field is then slightly larger, namely by the amount $B_{int} - B_{mext} = \mu_0 J_c\, w$ where J_c is the critical current density at the given temperature and magnetic field and w the wall thickness. Under the assumption $B_{int} - B_{ext} \ll B_{ext}$ both field and current density are almost constant throughout the wall. The reduction in well depth ΔU is proportional to the product of these quantities. If a bundle of flux quanta is released from its well, it will 'slide' down the slope and leave the material. In this way space is created for some magnetic flux from the bore of the cylinder which will migrate into the conductor and refill the well. As a consequence the internal field decreases and with it the critical current density in the wall. Its time derivative is roughly given by the expression

$$\frac{dJ_c}{dt} \approx -C \exp\left(\frac{\Delta U}{k_B T}\right) \approx -C \exp\left(\frac{\Phi_{av} a J_c l}{k_B T}\right) \tag{41}$$

where C is a constant. The solution of this unusual differential equation is

$$J_c(t) = J_c(0) - \frac{k_B T}{\Phi_{av} a\, l} \ln t\ . \tag{42}$$

This result implies that for given temperature and magnetic field the critical current density is not really a constant but depends slightly on time. What one usually quotes as J_c is the value obtained after the decay rate on a linear time scale has become unmeasurably small.

A nearly logarithmic time dependence is also observed in the persistent-current multipole fields of accelerator magnets, see e.g. [31]. So it seems tempting to attribute the effect to flux creep. Surprisingly, the decay rates are generally much larger than typical flux creep rates and depend moreover on the maximum field level in a preceding excitation, see Fig. 43a.

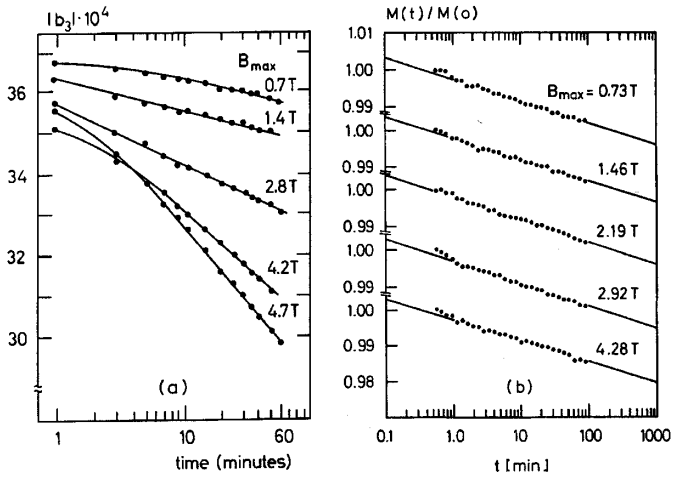

Fig. 43: (a) Decay of the sextupole coefficient in a HERA dipole at a field of 0.23 T for different values of the maximum field in the initialising cycle $0 \rightarrow B_{max} \rightarrow 0.04$T $\rightarrow$ 0.23 T [32]. (b) Magnetisation decay at zero field in a long sample of HERA cable for different values of the maximum field in the initialising cycle $0 \rightarrow B_{max} \rightarrow 0$ [33].

In cable samples this is not the case as is evident from Fig. 43b. The average magnetisation of a 5 m-long cable sample decays at low field ($B = 0$ in this case) by less than 1% per decade of time, and the decay rate is totally independent of the maximum field B_{max} in the preceding cycle. The observed rate agrees well with other data on flux creep in NbTi.

From the data in Fig. 43 it is obvious that thermally activated flux creep can explain only part of the time dependence of multipoles in magnets. The decay rates measured in magnets are usually much larger than those in cable samples, and there is a considerable variation from magnet to magnet. In 1995 experimental results [34] and model calculations [35] were presented showing that the time dependence is due to a complex interplay between magnetisation currents in the NbTi filaments and eddy currents among the strands of the cable. Quantitative predictions are not possible because of too many unknown parameters. For a more detailed discussion see [31].

Flux creep has become an important issue after the discovery of high-temperature superconductors. Figure 44 shows that the magnetisation of YBaCuO samples decays rapidly, in particular for single crystals. One speaks of ‘giant flux creep’. This is a strong hint that flux pinning is insufficient at 77 K and implies that the presently available materials are not yet suited for building magnets cooled by liquid nitrogen.

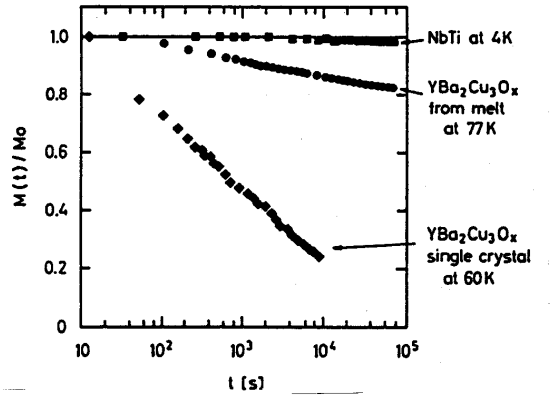

Fig. 44: Comparison of superconductor magnetisation decay due to flux creep in NbTi at a temperature of 4.2 K, in oriented-grained $YBa_2Cu_3O_x$ at 77 K and in a $YBa_2Cu_3O_x$ single crystal at 60 K [36].

7. SUPERCONDUCTORS IN MICROWAVE FIELDS

Superconductivity in microwave fields is not treated adequately in standard text books. For this reason I present in this section a simplified explanation of the important concepts. A similar treatment can be found in [37]. Superconductors are free from energy dissipation in direct-current (dc) applications, but this is no longer true for alternating currents (ac) and particularly not in microwave fields. The reason is that the high-frequency magnetic field penetrates a thin surface layer and induces oscillations of the electrons which are not bound in Cooper pairs. The power dissipation caused by the motion of the unpaired electrons can be characterized by a surface resistance. In copper cavities the surface resistance is given by

$$R_{surf} = \frac{1}{\delta\sigma} \tag{43}$$

where δ is the skin depth and σ the conductivity of the metal.

The response of a superconductor to an ac field can be understood in the framework of the *two-fluid model* [4]. An ac current in a superconductor is carried by Cooper-pairs (the superfluid component) as well as by unpaired electrons (the normal component). Let us study the response to a periodic electric field. The normal current obeys Ohm's law

$$J_n = \sigma_n \, E_0 \, \exp(-i\omega t) \tag{44}$$

while the Cooper pairs receive an acceleration $m_c \, \dot{v}_c = -2e \, E_0 \, \exp(-i\omega t)$, so the supercurrent density becomes

$$J_s = i \, \frac{n_c \, 2 \, e^2}{m_e \omega} E_0 \, \exp(-i\omega t) \; . \tag{45}$$

If we write for the total current density

$$J = J_n + J_s = \sigma E_0 \exp(-i\omega t) \tag{46}$$

[4] A similar model is used to explain the unusual properties of liquid helium below 2.17 K in terms of a normal and a superfluid component.

we get a complex conductivity:

$$\sigma = \sigma_n + i\sigma_s \quad \text{with} \quad \sigma_s = \frac{2\,n_c e^2}{m_e\,\omega} = \frac{1}{\mu_0 \lambda_L^2\,\omega}\ . \tag{47}$$

The surface resistance is the real part of the complex surface impedance

$$R_{surf} = Re\left(\frac{1}{\lambda_L(\sigma_n + i\sigma_s)}\right) = \frac{1}{\lambda_L}\cdot\frac{\sigma_n}{\sigma_n^2 + \sigma_s^2}\ . \tag{48}$$

Since $\sigma_n^2 \ll \sigma_s^2$ at microwave frequencies one can disregard σ_n^2 in the denominator and obtains $R_{surf} \propto \sigma_n/(\lambda_L\sigma_s^2)$. So we arrive at the surprising result that the microwave surface *resistance* is proportional to the normal-state *conductivity*.

The conductivity of a normal metal is given by the classic Drude expression

$$\sigma_n = \frac{n_n e^2 \ell}{m_e v_F} \tag{49}$$

where n_n is the density of the unpaired electrons, ℓ their mean free path and v_F the Fermi velocity. The normal electrons are created by thermal breakup of Cooper pairs. There is an energy gap $E_g = 2\Delta(T)$ between the BCS ground state and the free electron states. By analogy with the conductivity of an intrinsic (undoped) semiconductor we get

$$\sigma_n \ \propto\ \ell\,\exp(-E_g/(2k_BT)) = \ell\,\exp(-\Delta(T)/(k_BT))\ . \tag{50}$$

Using $1/\sigma_s = \mu_0\lambda_L^2\omega$ and $\Delta(T) \approx \Delta(0) = 1.76 k_B T_c$ we finally obtain for the BCS surface resistance

$$R_{BCS} \ \propto\ \lambda_L^3\,\omega^2\,\ell\,\exp(-1.76\,T_c/T)\ . \tag{51}$$

This formula displays two important aspects of microwave superconductivity: the surface resistance depends exponentially on temperature, and it is proportional to the square of the radio frequency.

Eq. (51) applies if the mean free path ℓ of the unpaired electrons is much larger than the coherence length ξ. In niobium this condition is usually not fulfilled and one has to replace λ_L in the above equation by [38]

$$\Lambda = \lambda_L\sqrt{1 + \xi/\ell}\ . \tag{52}$$

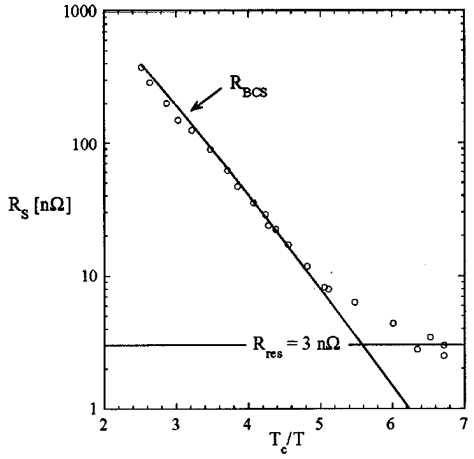

Fig. 45: The surface resistance of a 9-cell TESLA cavity plotted as a function of T_c/T. The residual resistance of 3 nΩ corresponds to a quality factor $Q_0 = 10^{11}$.

Combining equations (51) and (52) we arrive at the surprising statement that the surface resistance does not assume its minimum value when the superconductor is of very high purity ($\ell \gg \xi$) but rather in the range $\ell \approx \xi$. Experimental results [39] and theoretical models [40] confirm this prediction. The effect is also observed in copper cavities with a thin niobium sputter coating in which the electron mean free path is in the order of ξ. At 4.2 K the quality factors in the LEP cavities are indeed a factor of two higher than in pure niobium cavities [41].

In addition to the BCS term there is a residual resistance caused by impurities, frozen-in magnetic flux or lattice distortions.

$$R_{surf} = R_{BCS} + R_{res} \ . \tag{53}$$

R_{res} is temperature independent and amounts to a few nΩ for a clean niobium surface but may readily increase if the surface is contaminated.

For niobium the BCS surface resistance at 1.3 GHz amounts to about 800 nΩ at 4.2 K and drops to 15 nΩ at 2 K, see Fig. 45. The exponential temperature dependence is the reason why operation at 2 K is essential for achieving high accelerating gradients in combination with very high quality factors. Superfluid helium is an excellent coolant owing to its high heat conductivity.

8. JOSEPHSON EFFECTS

In 1962 B.D. Josephson made a theoretical analysis of the tunneling of Cooper pairs through a thin insulating layer from one superconductor to another and predicted two fascinating phenomena which were fully confirmed by experiment. A schematic experimental arrangement is shown in Fig. 46.

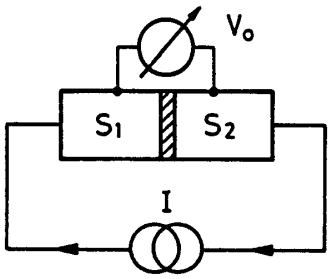

Fig. 46: Schematic arrangement for studying the properties of a Josephson junction.

DC Josephson effect. If the voltage V_0 across the junction is zero there is a dc Cooper-pair current which can assume any value in the range

$$-I_0 < I < I_0$$

where I_0 is a maximum current that depends on the Cooper-pair densities and the area of the junction.

AC Josephson effect. Increasing the voltage of the power supply eventually leads to a non-vanishing voltage across the junction and then a new phenomenon arises: besides a dc current which however is now carried by single electrons there is an alternating Cooper-pair current

$$I(t) = I_0 \sin(2\pi f_J t + \varphi_0) \tag{54}$$

whose frequency, the so-called *Josephson frequency*, is given by the expression

$$f_J = \frac{2eV_0}{2\pi\hbar} \ . \tag{55}$$

For a voltage $V_0 = 1\,\mu$V one obtains a frequency of 483.6 MHz. The quantity φ_0 is an arbitrary phase. Equation (55) is the basis of extremely precise voltage measurements.

8.1 Schrödinger equation of the Josephson junction

The wave functions in the superconductors 1 and 2 are called ψ_1 and ψ_2. Due to the possibility of tunneling through the barrier the two Schrödinger equations are coupled

$$i\hbar\frac{\partial\psi_1}{\partial t} = E_1\psi_1 + K\psi_2\,, \qquad i\hbar\frac{\partial\psi_2}{\partial t} = E_2\psi_2 + K\psi_1\,. \tag{56}$$

The quantity K is the coupling parameter. The macroscopic wave functions can be expressed through the Cooper-pair densities n_1, n_2 and the phase factors

$$\psi_1 = \sqrt{n_1}\exp(i\varphi_1)\,, \quad \psi_2 = \sqrt{n_2}\exp(i\varphi_2)\,. \tag{57}$$

We insert this into (56) and obtain

$$\left(\frac{\dot{n}_1}{2\sqrt{n_1}} + i\sqrt{n_1}\dot{\varphi}_1\right)\exp(i\varphi_1) = -\frac{i}{\hbar}[E_1\sqrt{n_1}\exp(i\varphi_1) + K\sqrt{n_2}\exp(i\varphi_2)]$$

and

$$\left(\frac{\dot{n}_2}{2\sqrt{n_2}} + i\sqrt{n_2}\dot{\varphi}_2\right)\exp(i\varphi_2) = -\frac{i}{\hbar}[E_2\sqrt{n_2}\exp(i\varphi_2) + K\sqrt{n_1}\exp(i\varphi_1)]\,.$$

Now we multiply these equation with $\exp(-i\varphi_1)$ resp. $\exp(-i\varphi_2)$ and separate the real and imaginary parts:

$$\begin{aligned}
\dot{n}_1 &= \frac{2K}{\hbar}\sqrt{n_1 n_2}\,\sin(\varphi_2-\varphi_1)\,,\\
\dot{n}_2 &= \frac{2K}{\hbar}\sqrt{n_1 n_2}\,\sin(\varphi_1-\varphi_2) = -\dot{n}_1\,,\\
\dot{\varphi}_1 &= -\frac{1}{\hbar}\left[E_1 + K\sqrt{\frac{n_2}{n_1}}\cos(\varphi_2-\varphi_1)\right]\,,\\
\dot{\varphi}_2 &= -\frac{1}{\hbar}\left[E_2 + K\sqrt{\frac{n_1}{n_2}}\cos(\varphi_1-\varphi_2)\right]\,.
\end{aligned} \tag{58}$$

For simplicity we consider the case where the two superconductors are identical, so $n_2 = n_1$. The Cooper-pair energies E_1 and E_2 differ by the energy gained upon crossing the voltage V_0 :

$$E_2 = E_1 - 2eV_0\,.$$

The equations simplify

$$\begin{aligned}
\dot{n}_1 &= \frac{2K}{\hbar}n_1\sin(\varphi_2-\varphi_1) = -\dot{n}_2\,,\\
\frac{d}{dt}(\varphi_2-\varphi_1) &= -\frac{1}{\hbar}(E_2-E_1) = \frac{2eV_0}{\hbar}\,.
\end{aligned} \tag{59}$$

Integrating the second equation (59) yields the Josephson frequency

$$\varphi_2(t) - \varphi_1(t) = \frac{2eV_0}{\hbar}\cdot t + \varphi_0 = 2\pi f_J\cdot t + \varphi_0\,. \tag{60}$$

The Cooper-pair current through the junction is proportional to $\dot{n}_1$. Using (59) and (60) it can be written as

$$I(t) = I_0\sin\left(\frac{2eV_0}{\hbar}\,t + \varphi_0\right)\,. \tag{61}$$

There are two cases:
(1) For zero voltage across the junction we get a dc current

$$I = I_0\sin\varphi_0$$

which can assume any value between $-I_0$ and $+I_0$ since the phase φ_0 is not specified.
(2) For $V_0 \neq 0$ there is an ac Cooper–pair current with exactly the Josephson frequency.

8.2 Superconducting quantum interference

A loop with two Josephson junctions in parallel (Fig. 47) exhibits interference phenomena that are similar to the optical diffraction pattern of a double slit. Assuming zero voltage across the junctions the total current is

$$I = I_a + I_b = I_0(\sin\varphi_a + \sin\varphi_b) \ .$$

When a magnetic flux $\Phi_{\rm mag}$ threads the area of the loop, the phases differ according to Sec. 5 by

$$\varphi_b - \varphi_a = \frac{2e}{\hbar}\oint \vec{A}\cdot\vec{ds} = \frac{2e}{\hbar}\Phi_{mag} \ .$$

With $\varphi_0 = (\varphi_a + \varphi_b)/2$ we get

$$\varphi_a = \varphi_0 + \frac{e}{\hbar}\Phi_{mag}, \quad \varphi_b = \varphi_0 - \frac{e}{\hbar}\Phi_{mag}$$

and the current is

$$I = I_0 \sin\phi_0 \ \cos\left(\frac{e}{\hbar}\Phi_{mag}\right) \ . \tag{62}$$

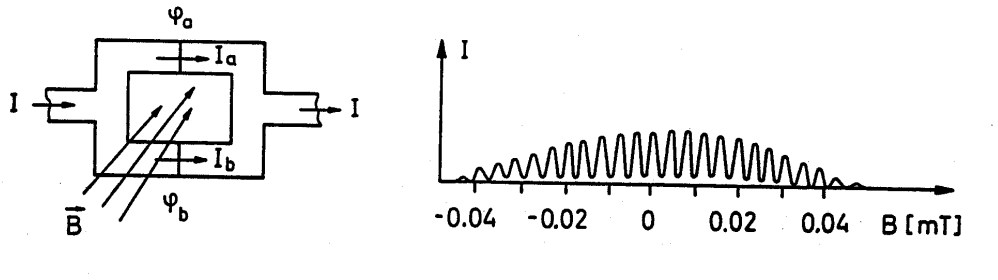

Fig. 47: A loop with two Josephson junctions and the observed interference pattern [42]. The amplitude modulation is caused by the fi nite width of the junctions.

As a function of the magnetic flux one obtains a typical double-slit interference pattern as shown in Fig. 47. Adjacent peaks are separated by one flux quantum $\Delta\Phi_{mag} = \Phi_0$, so by counting flux quanta one can measure very small magnetic fields. This is the basic principle of the Superconducting Quantum Interference Device (SQUID). Technically one often uses superconducting rings with a single weak link which acts as a Josephson junction. Flux transformers are applied to increase the effective area and improve the sensitivity.

A FREE ENERGY IN THERMODYNAMICS

To illustrate the purpose of the free energy I consider first an ideal gas. The internal energy is the sum of the kinetic energies of all atoms

$$U = \sum_{i=1}^{N} \frac{m}{2} v_i^2 = \frac{3}{2}\, N\, k_B T \tag{63}$$

and depends only on temperature but not on volume. The first law of thermodynamics describes energy conservation:

$$dU = \delta Q + \delta W \ . \tag{64}$$

The internal energy increases either by adding heat δQ or mechanical work $\delta W = -p\,dV$ to the gas. For a reversible process one has $\delta Q = T\,dS$ where S is the entropy. Now consider an isothermal expansion of the gas. Thereby the gas transforms heat into mechanical work:

$$dU = 0 \quad \text{for} \quad T = \text{const} \quad \Rightarrow \quad \delta Q = -\delta W = p\,dV\ . \tag{65}$$

The gas produces mechanical work but its internal energy does not change, hence U is not an adequate variable to describe the process. What is the correct energy variable? We will see that this is the Helmholtz free energy, given by

$$F = U - T\,S \quad \Rightarrow \quad dF = dU - SdT - TdS = \delta W - SdT\ . \tag{66}$$

For an isothermal expansion ($dT = 0$) we get $dF = \delta W$, i.e. $-dF = pdV$: the work produced by the gas is identical to the reduction of its free energy.

Now we consider a magnetic material of permeability μ inside a coil which generates a field H. The magnetization is $\vec{M} = (\mu - 1)\vec{H}$. Its potential energy (per unit volume) in the magnetic field is

$$E_{pot} = -\mu_0\,\vec{M}\cdot\vec{H}\ . \tag{67}$$

If the magnetization changes by $d\vec{M}$ the work is $\delta W = \mu_0\,d\vec{M}\cdot\vec{H}$. Defining again the Helmholtz free energy by eq. (66) we get by analogy with the ideal gas $dF = \delta W$, hence F can in fact be used to describe the thermodynamics of magnetic materials in magnetic fields. One drawback is, however, that the magnetization of a substance cannot be directly varied by the experimenter. What can be varied at will is the magnetic field H, namely by choosing the coil current. For this reason another energy function is more appropriate, the Gibbs free energy

$$G = F - \mu_0\,\vec{M}\cdot\vec{H} = U - T\,S - \mu_0\,\vec{M}\cdot\vec{H}\ . \tag{68}$$

For an isothermal process we get $dG = -\mu_0\,\vec{M}\cdot d\vec{H}$. Let us apply this to a superconductor in the Meissner phase. Then $\mu = 0$ and $\vec{M} = -\vec{H}$ from which follows

$$dG_{sup} = \mu_0\,M(H)dH = \frac{\mu_0}{2}\,d(H^2) \ \Rightarrow\ G_{sup}(H) = G_{sup}(0) + \frac{\mu_0}{2}\,H^2\ . \tag{69}$$

This equation is used in Sect. 3.

B THE FORMATION OF A COOPER PAIR

To illustrate the spirit of the BCS theory I will present the mathematics of Cooper-pair formation. Let us consider a metal at $T = 0$. The electrons fill all the energy levels below the Fermi energy while all levels above E_F are empty. The wave vector and the momentum of an electron are related by

$$\vec{p} = \hbar\vec{k}\ .$$

In the three-dimensional k space the Fermi sphere has a radius $k_F = \sqrt{2m_eE_F}/\hbar$. To the fully occupied Fermi sphere we add two electrons of opposite wave vectors $\vec{k}_1 = -\vec{k}_2$ whose energy $E_1 = E_2 = \hbar^2k_1^2/(2m_e)$ is within the spherical shell (see Figs. 20, 23)

$$E_F < E_1 < E_F + \hbar\omega_D\ . \tag{70}$$

From Sect. 4 we know that $\hbar\omega_D$ is the largest energy quantum of the lattice vibrations. The interaction with the 'sea' of electrons inside the Fermi sphere is neglected except for the Pauli Principle: the two additional electrons are forbidden to go inside because all levels below E_F are occupied. Under this assumption the two electrons together have the energy $2E_1 > 2E_F$. Now the attractive force provided

by the lattice deformation is taken into consideration. Following Cooper [18] we must demonstrate that the two electrons then form a bound system, a 'Cooper pair', whose energy drops below twice the Fermi energy

$$E_{pair} = 2E_F - \delta E < 2E_F \ .$$

The Schrödinger equation for the two electrons reads

$$-\frac{\hbar^2}{2m_e}(\nabla_1^2 + \nabla_1^2)\,\psi(\vec{r}_1,\vec{r}_2) + V(\vec{r}_1,\vec{r}_2)\psi(\vec{r}_1,\vec{r}_2) = E_{pair}\psi(\vec{r}_1,\vec{r}_2) \tag{71}$$

where V is the interaction potential due to the dynamical lattice polarisation. In the simple case of vanishing interaction, $V = 0$, the solution of (71) is the product of two plane waves

$$\psi(\vec{r}_1,\vec{r}_2) = \frac{1}{\sqrt{L^3}}\exp(i\vec{k}_1\cdot\vec{r}_1)\cdot\frac{1}{\sqrt{L^3}}\exp(i\vec{k}_2\cdot\vec{r}_2) = \frac{1}{L^3}\exp(i\vec{k}\cdot\vec{r})$$

with $\vec{k}_1 = -\vec{k}_2 = \vec{k}$ the k-vector, $\vec{r} = \vec{r}_1 - \vec{r}_2$ the relative coordinate and L^3 the normalisation volume. The most general solution of Eq. (71) with $V = 0$ is a superposition of such functions

$$\psi(\vec{r}) = \frac{1}{L^3}\sum_{\vec{k}} g(\vec{k})\exp(i\vec{k}\cdot\vec{r}) \tag{72}$$

with the restriction that the coefficients $g(\vec{k})$ vanish unless $E_F \le \hbar^2k^2/2m_e \le E_F + \hbar\omega_D$. This function is certainly not an exact solution of the equation (71) with $V \neq 0$ but for a weak potential it can be used to obtain the energy E_{pair} in first order perturbation theory. For this purpose we insert (72) into Eq. (71):

$$\frac{1}{L^3}\sum_{\vec{k}'} g(\vec{k}')\left[\frac{\hbar^2k'^2}{m_e} + V(\vec{r}) - E_{pair}\right]\exp(i\vec{k}'\cdot\vec{r}) = 0\ .$$

This equation is multiplied by $\exp(-i\vec{k}\cdot\vec{r})$ and integrated, using the orthogonality relations

$$\frac{1}{L^3}\int\exp\left(i(\vec{k}'-\vec{k})\cdot\vec{r}\right)d^3r = \delta_{\vec{k}\vec{k}'} \quad \text{with} \ \ \delta_{\vec{k}\vec{k}'} = \begin{cases} 1 \text{ for } \vec{k} = \vec{k}' \\ 0 \text{ otherwise}\,. \end{cases}$$

Introducing further the transition matrix elements of the potential V

$$V_{\vec{k}\vec{k}'} = \int\exp\left(-i(\vec{k}-\vec{k}')\cdot\vec{r}\right)\,V(\vec{r})d^3r \tag{73}$$

one gets a relation among the coefficients of the expansion (72)

$$g(\vec{k})\left[\frac{\hbar^2k^2}{m_e} - E_{pair}\right] = -\frac{1}{L^3}\sum_{\vec{k}'} g(\vec{k}')V_{\vec{k}\vec{k}'}\ . \tag{74}$$

The matrix element $V_{\vec{k}\vec{k}'}$ describes the transition from the state $(\vec{k},-\vec{k})$ to any other state $(\vec{k}',-\vec{k}')$ in the spherical shell of thickness $\hbar\omega_D$ around the Fermi sphere. Cooper and later Bardeen, Cooper and Schrieffer made the simplest conceivable assumption on these matrix elements, namely that they are all equal.

$$V_{\vec{k}\vec{k}'} = -V_0 \quad \text{for} \quad E_F < \frac{\hbar^2k^2}{2m_e}, \frac{\hbar^2k'^2}{2m_e} < E_F + \hbar\omega_D \tag{75}$$

and $V_{\vec{k}\vec{k}'} = 0$ elsewhere. The negative value ensures attraction. With this extreme simplification the right-hand side of Eq. (74) is no longer $\vec{k}$ dependent but becomes a constant

$$-\frac{1}{L^3}\sum_{\vec{k}'} g(\vec{k}')V_{\vec{k}\vec{k}'} = \frac{V_0}{L^3}\sum_{\vec{k}'} g(\vec{k}') = A\,. \tag{76}$$

Then Eq. (74) yields for the coefficients

$$g(\vec{k}) = \frac{A}{\hbar^2k^2/m_e - E_{pair}} = \frac{A}{\hbar^2k^2/m_e - 2E_F + \delta E}\,.$$

The constant A is still unknown. We can eliminate it by summing this expression over all $\vec{k}$ and using (76) once more

$$\sum_{\vec{k}} g(\vec{k}) = A\frac{L^3}{V_0}$$

from which follows

$$A\,\frac{L^3}{V_0} = \sum_{\vec{k}} \frac{A}{\hbar^2k^2/m_e - 2E_F + \delta E}\,.$$

Dividing by A leads to the important consistency relation

$$1 = \frac{V_0}{L^3}\sum_{\vec{k}} \frac{1}{\hbar^2k^2/m_e - 2E_F + \delta E}\,. \tag{77}$$

The sum extends over all $\vec{k}$ vectors in the shell between E_F and $E_F + \hbar\omega_D$. Since the states are very densely spaced one can replace the summation by an integration

$$\frac{1}{L^3}\sum_{\vec{k}} \to \frac{1}{(2\pi)^3}\int d^3k \to \int \mathcal{N}(E)dE$$

where $\mathcal{N}(E)$ is the density of single-electron states for a definite spin orientation. (The states with opposite spin orientation must not be counted because a Cooper pair consists of two electrons of opposite spin). The integration spans the narrow energy range $[E_F, E_F + \hbar\omega_D]$ so $\mathcal{N}(E)$ can be replaced by $\mathcal{N}(E_F)$ and taken out of the integral. Introducing a scaled energy variable

$$\xi = E - E_F = \frac{\hbar^2k^2}{2m_e} - E_F$$

formula (77) becomes

$$1 = V_0\,\mathcal{N}(E_F)\int_0^{\hbar\omega_D} \frac{d\xi}{2\xi + \delta E}\,. \tag{78}$$

The integral yields

$$\frac{1}{2}\ln\left(\frac{\delta E + 2\hbar\omega_D}{\delta E}\right)\,.$$

The energy shift is then

$$\delta E = \frac{2\hbar\omega_D}{\exp(2/(V_0\,\mathcal{N}(E_F)) - 1}\,.$$

For small interaction potentials ($V_0\mathcal{N}(E_F) \ll 1$) this leads to the famous Cooper formula

$$\delta E = 2\hbar\omega_D \exp\left(-\frac{2}{V_0\,\mathcal{N}(E_F)}\right)\,. \tag{79}$$

Except for a factor of 2 the same exponential appears in the BCS equations for the energy gap and the critical temperature.

References

[1] W. Buckel, *Supraleitung*, 4. Auflage, VCH Verlagsgesellschaft, Weinheim 1990

[2] D.R. Tilley & J. Tilley, *Superfluidity and Superconductivity*, Third Edition, Institute of Physics Publishing Ltd, Bristol 1990

[3] H.K. Onnes, Akad. van Wetenschappen (Amsterdam) **14**, 113, 818 (1911)

[4] J. File and R.G. Mills, Phys. Rev. Lett. **10**, 93 (1963)

[5] M.N. Wilson, private communication

[6] W. Meissner and R Ochsenfeld, Naturwiss. **21**, 787 (1933)

[7] F. London and H. London, Z. Phys. **96**, 359 (1935)

[8] J. Bardeen, L.N. Cooper and J.R. Schrieffer, Phys. Rev. **108**, 1175 (1957)

[9] V.L. Ginzburg and L.D. Landau, JETP USSR **20**, 1064 (1950)

[10] L.P. Gorkov, Sov. Phys. JETP **9**, 1364 (1960), JETP **10**, 998 (1960)

[11] A.A. Abrikosov, Sov. Phys. JETP **5**, 1174 (1957)

[12] U. Essmann and H. Träuble, Phys. Lett. **24A**, 526 (1967) and Sci. Am. **224**, March 1971

[13] B.D. Josephson, Phys. Rev. Lett. **1**, 251 (1962)

[14] J.D. Livingston, Phys. Rev. **129**, 1943 (1963)

[15] N.E. Phillips, Phys. Rev. **134**, 385 (1965)

[16] Th. Schilcher, Diploma Thesis, Hamburg 1994, unpublished

[17] M.N. Wilson, *Superconducting Magnets*, Oxford University Press 1997

[18] L.N. Cooper, Phys. Rev. **104**, 1189 (1956)

[19] H. Ibach and H. Lüth, *Solid State Physics*, 2nd Edition, Springer-Verlag, Berlin 1996

[20] Y. Aharonov and D. Bohm, Phys. Rev. **115**, 485 (1955)

[21] G. Möllenstedt and W. Bayh, Phys. Bl. **18**, 229 (1962)

[22] A. Tonomura, Phys. Today, April 1990

[23] R. Doll and M. Näbauer, Phys. Rev. Lett. **7**, 51 (1961)

[24] B.S. Deaver and W.M. Fairbank, Phys. Rev. Lett. **7**, 43 (1961)

[25] H. Rietschel, Phys. Bl. **46**, 419 (1990)

[26] C.E. Gough et al., Nature **326**, 855 (1987)

[27] G.T. Lee et al., Physica C **161**, 195 (1989)

[28] Y.B. Kim, C.F. Hempstead and A.R. Strnad, Phys. Rev. **139**, A1163 (1965)

[29] Y.B. Kim, C.F. Hempstead and A.R. Strnad, Phys. Rev. Lett. **9**, 306 (1962)

[30] P.W. Anderson, Phys. Rev. Lett. **9**, 309 (1962)

[31] K.-H. Mess, P. Schmüser, S. Wolff, *Superconducting Accelerator Magnets*, World Scientific, Singapore, 1996

[32] H. Brück et al., Contribution to the European Accelerator Conference, Nice 1990

[33] M. Halemeyer et al., IEEE Trans. Appl. Supercond. Vol.3, No.1, 168 (1993)

[34] A.P. Verweij and H.H.J. ten Kate, IEEE Trans. **ASC-5** (1995) 404

[35] L. Krempaski and C. Schmidt, Appl. Phys. Lett. **66** (1995) 1545, and J. Appl. Phys. **78** (1995) 5800

[36] C. Keller et al., Cryogenics **30**, 410 (1990)

[37] H. Padamsee, J. Knobloch and T. Hays, *RF Superconductivity for Accelerators*, John Wiley, New York 1998

[38] B. Bonin, CERN Accelerator School *Superconductivity in Particle Accelerators*, CERN 96-03, ed. S. Turner, Hamburg (1995)

[39] F. Palmer, Proc. 3rd Workshop on RF Superconductivity, K. Shephard (ed.), Argonne Natl. Lab. 1988, p. 309

[40] J. Halbritter, Z. Physik **238** (1970) 466

[41] C. Benvenuti *et al.*, Proc. PAC91, San Francisco (1991), p. 1023.

[42] R.C. Jaklevic et al. Phys. Rev. **140**, A1628 (1965)